Fourier Transform Infrared Spectroscopy (FTIR) Analysis of Silicon Carbide Nanowires

A thesis submitted to the
Graduate School of Natural and Applied Sciences

by

Dilhumar ABDURAZIK

in partial fulfillment for the
degree of Master of Science

in

Industrial and Systems Engineering

This is to certify that we have read this thesis and that in our opinion it is fully adequate, in scope and quality, as a thesis for the degree of Master of Science in Industrial and Systems Engineering.

APPROVED BY:

Assoc. Prof. Dr. Kasif Teker .....
(Thesis Advisor)

Prof. Dr. Orhan Şahin .....

Asst. Prof. Dr. M. Kemal. Özdemir .....

This is to confirm that this thesis complies with all the standards set by the Graduate School of Natural and Applied Sciences of Istanbul Sehir University:

DATE OF APPROVAL:

SEAL/SIGNATURE:

Declaration of Authorship

I, Dilhumar ABDURAZIK, declare that this thesis titled, 'Fourier Transform Infrared Spectroscopy (FTIR) Analysis of Silicon Carbide Nanowires ' and the work presented in it are my own. I confirm that:

- This work was done wholly or mainly while in candidature for a research degree at this University.
- Where any part of this thesis has previously been submitted for a degree or any other qualification at this University or any other institution, this has been clearly stated.
- Where I have consulted the published work of others, this is always clearly attributed.
- Where I have quoted from the work of others, the source is always given. With the exception of such quotations, this thesis is entirely my own work.
- I have acknowledged all main sources of help.
- Where the thesis is based on work done by myself jointly with others, I have made clear exactly what was done by others and what I have contributed myself.

Signed: دىلھۇمار ئابدۇرازىق

Date: 3 May 2016

Fourier Transform Infrared Spectroscopy (FTIR) Analysis of Silicon Carbide Nanowires

Dilhumar Abdurazik

Abstract

Silicon carbide (SiC) nanowires have attracted particular research enthusiasm for their favorable applications in nanoscale optoelectronics, sensors, high frequency, high temperature, and high-power electronics. A comprehensive Fourier transform infrared spectroscopy (FTIR) analysis of the SiC nanowires has been conducted. FTIR gives very important and practical information about the chemical bond states of materials. FTIR studies showed three strong peaks at the spectrum, which can be assigned to SiC transverse optical (TO) mode, SiC longitudinal optical (LO) mode, and Si-O stretching mode. Further, the differences of phonon states of SiC nanowires compared to the bulk SiC have been discussed. The Si-C TO stretching absorption band ranges from 783 cm^{-1} to 793 cm^{-1} with the full width at half maximum (FWHM) values from 21 cm^{-1} to 36 cm^{-1} with Fe-film catalyst, while the Si-C TO stretching absorption band ranges from 782 cm^{-1} to 784 cm^{-1} with the FWHM values from 13 $cm^{-1}$to 31 cm^{-1} with Ni-film catalyst. The FWHM values of the TO mode absorption of the SiC nanowires are significantly lower than that of bulk SiC (FWHM 59 cm^{-1}) suggesting higher bond quality and uniformity of the SiC nanowires. Moreover, the SiC TO mode absorption shifted towards the lower wavenumber region compared to the wavenumber of bulk single crystal SiC (800 cm^{-1}). These results show that FTIR provides quick and valuable information about the chemical bond states, crystal structure, and crystal quality of the nanostructured materials. Additionally, a practical synthesis method for SiC nanowire fabrication has been discussed; and morphology and crystal structure investigation of the SiC nanowires grown with various catalyst materials has been provided.

Keywords: Fourier transform infrared spectroscopy, SiC nanowires, Chemical vapor deposition, High temperature electronics, Nanomanufacturing

Fourier Transform ile Silisyum Karbür Nanotellerinin Kızılötesi Spektroskopi Analizi

Dilhumar Abdurazik

Öz

Silisyum karbür nanotelleri, olumlu uygulamalarından dolayı araştırma için cazibe merkezi haline gelmiştir. Bu olumlu uygulamaları nano optoelektronik, sensörler, yüksek frekans, yüksek sıcaklık ve yüksek güç elektroniği diye ayırabiliriz. Bu çalışmada SiC nanotellerinin kapsamlı bir Fourier transforumu kızılötesi spektroskopi (FTIR) analizi yapılmıştır. FTIR, materyallerin kimyasal bağlarının durumu hakkında önemli ve pratik bilgiler verir. FTIR çalışmaları specktrumda üç tane güçlü tepe noktası olduğunu göstermiştir. Bu tepe noktaları SiC enine optik (TO) modu, SiC boyuna optik (LO) modu ve Si-O esneme modu olarak üçe ayrılır. Ayrıca, kitle SiC ve SiC nanotellerinin fonon durumlarının farkları ele alınmıştır. Ni-film katalizörlü, 13 cm^{-1} ile 31 cm^{-1} arasında değer alan yarı-doruk genişliğine (FWHM) sahip Si-C TO germe emilim genişliği 782 cm^{-1} ile 784 cm^{-1} arasında değişmekteyken; Fe-film katalizörlü, 21 cm^{-1} ile 36 cm^{-1} arasında değer alan yarı-doruk genişliğine (FWHM) sahip Si-C TO germe emilim genişliği 783 cm^{-1} ile 793 cm^{-1} arasında değişmektedir. SiC nanotellerinin TO mod emilimi kitle SiC (FWHM 59 cm^{-1}) mod emiliminden önemli derecede küçüktür. Bu durum SiC nanotellerinin yüksek tahvil kalitesi ve tutarlılığı olduğunu göstermektedir. Buna ek olarak, toplu tek kristal SiC (800 cm^{-1}) dalga sayısı SiC TO mod emilimi karşılaştırıldığında, SiC TO mod emilimi küçök dalga sayısı olan bölgeye doğru kaymaktadır. Bütün bu sonuçlar şunu göstermektedir; FTIR nano yapılı materiyallerin kimyasal bağlarının durumu, kristal yapısı ve kristal kalitesi hakkında hızlı ve değerli bilgiler verir. Bunlara ilave olarak, SiC nanotel üretimi için pratik bir sentez yöntemi ele alınmış ve çeşitli katalizör malzemeler ile yetiştirilen SiC nanotellerinin morfolojisi ve kristal yapısı incelenmiştir.

Anahtar Sözcükler: Fourier transforumu kızılötesi spektroskopi, Silisyum Karbür, Kimyasal buhar depozisyon, Yüksek sıcaklık elektroniği, Nano üretim

Acknowledgments

The graduate study at Istanbul Sehir University has been very momentous and exciting. I would like to express my deep gratitude to many people, who have helped me a lot and made these years wonderful.

First of all, I am very grateful to my supervisor, Dr. Kasif Teker, for his continuous support, generous assistance, encouragements, valuable ideas and guidance during my graduate program and thesis work at Istanbul Sehir University. His patience, great broad view and kindness towards whole research has always been a great motivation to me in analyzing and solving complicated engineering and scientific problems. Thanks for giving his precious time and willingness to help on my thesis work.

I am also thankful to my peers, Ms. Zeynep and Mr. Amit, and all other graduate students in our department, who have always encouraged me throughout this thesis work. They have been always giving me useful suggestions and offering me their care.

Last but not least, I would like to express my deepest and sincerest appreciation to my parents and sisters for their patience, encouragement, love and providing me constant support throughout my life. They have been inspiring me at every moment.

Contents

List of Figures

List of Tables

Abbreviations

SiC	**S**ilicon **C**arbide
FTIR	**F**ourier **T**ransform **I**nfrared **S**pectroscopy
FWHM	**F**ull **W**idth at **H**alf **M**aximum
TEM	**T**ransmission **E**lectron **M**icroscopy
SEM	**S**canning **E**lectron **M**icroscopy
TO	**T**ransverse **O**ptical
LO	**L**ongitudinal **O**ptical
VLS	**V**apor - **L**iquid - **S**olid
SLS	**S**olid - **L**iquid - **S**olid
VS	**V**apor - **S**olid
FN	**F**owler - **N**ordheim
XRD	**X**-ray **D**iffraction
HMDS	**H**examethyldisilane
CNT	**C**arbon **N**anotubes
ACF	**A**ctivated **C**arbon **F**ibers
PL	**P**hotoluminescence
IR	**I**nfrared **R**adiation

Chapter 1

Introduction

1.1 Background

Silicon carbide (SiC), which is an essential wide band-gap semiconductor, exhibits properties such as excellent physical and chemical stability, high thermal conductivity, high saturation drift velocity, and high break down field strength. Recently, the wide application domains of SiC technologies have made functional SiC nanodevices a reality and resulted in a prominent promotion in the various SiC nanomaterial qualities. For instance, the commercial applications of SiC permit it to be used in optoelectronic devices such as light-emitting diodes and photodiodes. Besides, SiC is also widely applied in high-power devices, high-temperature sensors and electronics, as well as microwave devices owing to their excellent mechanical, electrical, optical, physical, and chemical properties [1].

It has been reported that SiC based one-dimensional nanostructures like nanorods, nanotubes, nanowhiskers, and nanowires have a number of unique properties and potential novel applications [2, 3]. SiC one-dimensional nanostructure is an encouraging candidate for strengthening phases in metal, polymer-matrix composites, ceramic, and optical applications due to their combination of particular mechanical, electronic, and superior chemical, physical stability, and their thermal properties. Due to the quantum confinement, low dimensionality, and shape effects, one-dimensional SiC nanostructures are supposed to demonstrate more excellent optical, mechanical, electronic, physical, and

chemical properties, which could offer new applications in microelectronics and photoelectronics. For instance, Zhu et al. reported a tunable violet–blue photoluminescence of SiC nanowires after the elimination of the SiO_2 shell [4]. Wang et al. observed 3C-SiC nanowires exhibiting a promising photocatalyst characterization [5]. Xu et al. discovered that SiC nanowires have superior superhydrophobic properties [6, 7]. Choi et al. produced diode-type field effect transistor devices made up by SiC-nanowire and exhibited marvelous field emission properties of SiC nanowires [8].

It has been demonstrated that the shape and crystallite size of semiconductor nanomaterials determine their chemical and physical properties. With decreasing of the crystallite size, quantum confinement exhibits its effect in widening of the band gap, and its implications on the photophysics of the crystallites and electronic structure have attracted considerable interest [9]. Consequently, the band gap characterization of semiconductor nanomaterials has also caught researchers' notice. Recently, there are comprehensive researches on the optical, electronic, and mechanical properties of SiC nanowires. However, there is a rare study on the band gap characterization of the SiC nanowires [10].

Nanowires are building blocks for the synthesis of all kinds of nanoscale devices [11–13]. In addition, physical and chemical properties of a nanowire are much superior compared to the bulk or thin film based on theoretical calculations [1]. SiC nanowires are desirable nanomaterials for designing and producing nanodevices due to their distinctive and excellent physical, chemical properties and unique advantages. Therefore, the production and comprehension of the various properties of SiC nanowires are significantly important for the improvement of the nanowire based nanodevices. In particular, the high electrical conductance and super mechanical properties of silicon carbide nanowires make them excellent candidates to be as nanocontacts in harsh environments or for the reinforcement of various nanocomposite materials. From the fundamental research standpoint, study on silicon carbide one dimensional nanowires would be emphasized for what concerns the potential application in nanocomposites and nanodevices.

A broad spectrum of applications are available due to the exciting new developments in SiC technology. Because of the field-emitting, unique mechanical, electronic, and hydrophobic properties and the promising applications of the SiC nanowires, it has been applied in fields such as hydrophobic and nanocomposites devices, electronic and optoelectronic nanodevices. For example, SiC nanowire field effect transistors are supposed to

be capable of running at higher temperatures compared to their Si-based counterparts. SiC nanowires also exhibit practical benefits for constructing field emission cathodes owing to their high aspect ratio, and they present excellent physical, chemical stability and low electron affinity value. Additionally, owing to the wonderful thermoelectric properties of SiC, thermoelectric applications of SiC nanowires are also very widely used [14]. Generally, SiC high-temperature devices offer promise in transmitters for deep well drilling, jet engine ignition systems, aircraft and automotive engine sensors, and a number of industrial process control and measurement systems. SiC high-power devices are developed for power supplies, surge suppressors, and solid-state lamp ballasts [15]. SiC high-frequency power devices are being applied in phased array radar systems, cellular phone base stations, high-frequency power supplies, small-lightweight radio frequency, and microwave transmitters [16].

1.2 Motivation

Due to the distinctive applications in the production of the nanoscale devices and the mesoscopic physics, all kinds of one-dimensional structures like oxide nanowires, semiconductor nanowires, and carbon nanotubes have become an important point of ongoing research. Among various nanowire materials, SiC nanowires have caught considerable interest nowadays because of their unique physical, chemical properties, and great potential for nano- and opto-electronics. It is well known that the size and shape of inorganic nanomaterials have a significant effect on their widely varying optical and electrical properties, which is significant in several applications, such as biological labeling, solar cells, catalysis, and light-emitting diodes.

As discussed earlier, SiC nanowires have been coming into great notice owing to their prominent properties such as high thermal conductivity and stability, high hardness, high break down field strength, high wear resistance, excellent chemical inertness, and mechanical properties. Therefore, it has been also recommended as splendid materials favorable to be utilized for the reinforcment of nanocomposites because of their strong interfacial bonding and much greater strength compared to their bulk counterparts. For example, it is observed that the largest bonding strengths and elastic modulus of SiC

nanorods with several tens of nanometers thick were 53.4 GPa and 610-660 GPa respectively, which was much higher than earlier observed data for SiC whiskers of micrometer diameter [17, 18].

SiC nanowires have been synthesized by many kinds of experimental setups employing different growth mechanisms. Every growth method shows special benefits and it is very complicated to draw conclusions that which experimental growth mechanisms lead to SiC nanowires in the best quality appropriate for all kinds of applications. The essential distinctions between all kinds of configuration mechanisms are related to the nanowire growth throughput, the dimension, the cost of the precursors, with or without metallic catalyst, the feasibility of preparative radial heterostructures, the required maximum temperature etc. But there are no significant distinctions among the growth mechanisms, where it involves the quality of individual nanowires crystallization.

This thesis aims at introducing the explanations of the different growth methods and various properties of SiC nanowires. To date, a lot of growth techniques have been developed to produce SiC nanowires, such as chemical vapor deposition technology, carbon nanotubes confined reaction, arc discharge technology, laser ablation technology, high-frequency induction heating technology, thermal evaporation method, metal-assisted vapor-liquid-solid (VLS) mechanism, vapor-solid (VS) mechanism, and solid-liquid-solid (SLS) mechanism. In our study, SiC nanowires were successfully synthesized on SiO_2/Si substrate by the low pressure chemical vapor deposition method via VLS mechanism with metal catalysts.

Generally, the phase composition, microstructure and morphology of the produced SiC nanowires were investigated by scanning electron microscopy (SEM), transmission electron microscopy (TEM), X-ray diffraction (XRD), energy dispersive spectroscopy, auger electron spectrum, and high-resolution transmission electron microscopy. In our report, the characteristics and crystallinity of synthesized SiC nanowires were mainly analyzed by TEM, SEM, FTIR spectroscopy, and XRD. Our analysis focus on FTIR, which is a useful method for investigating materials composition and microstructure. Infrared absorption spectroscopy is the subject of interaction of infrared radiation with matter as a function of photon frequency. FTIR gives concrete information relating molecular microstructures, the rotation and vibration of the chemical bonding states of materials, making it easier for investigating inorganic materials as well as organic materials. An

infrared spectrum provides a sample's fingerprint with absorption peaks, corresponding to the frequencies of vibrations between the chemical bonds of the atoms. Because each material has a unique atom combination, there are no two materials producing the exact same infrared spectrum. Thus, FTIR spectroscopy can identify unknown materials.

1.3 Overview

The objective of this thesis is to investigate FTIR characteristics of SiC nanowires grown at different temperatures with various catalyst materials by low pressure chemical vapor deposition.

In Chapter one, the background and advantages of silicon carbide nanowires are introduced. The objective of the thesis along with motivation are also included.

In Chapter two, concise information about SiC nanowires is introduced. The crystallographic structures, unique chemical, optical, electrical, and mechanical properties of SiC nanowires are described. Also, the growth method of SiC nanowires has been included in this chapter.

In Chapter three, the experimental details are described, including the techniques for the optical and structural characterizations, such as X-ray diffraction, transmission electron microscopy, scanning electron microscopy, and Fourier transform infrared spectroscopy. The experimental setup and procedures for the growth of SiC nanowires are described.

In Chapter four, the structural properties of SiC nanowires and growth condition are studied. Besides, XRD pattern of the SiC nanowires are discussed.

In Chapter five, FTIR characterization of the SiC nanowires is described. A comprehensive FTIR spectroscopy investigation of the SiC nanowires grown with various catalyst materials at different temperatures is provided.

In Chapter six, the thesis work is concluded and future work is discussed.

Chapter 2

Properties and Growth of SiC Nanowires

2.1 Crystallographic Structures of SiC

The wide band gap semiconductor SiC exists with many crystal structures, which are called polytypes. In spite of the point that all polytypes of SiC are chemically composed of 50% silicon atoms covalently bonded with 50% carbon atoms, every SiC polytype possesses different specific physical, chemical, and electrical properties. Although there are more than 200 known SiC polytypes in existence, only a small number of polytypes are usually capable of being reproduced suitably for applications in electronics. The polytypes can be obtained by different stacking layers in a unit cell. The most common SiC polytypes, which are now developed for electronic applications, are cubic (3C-SiC), the rhombohedral (15R-SiC), the hexagonal (2H-SiC, 4H-SiC and 6H-SiC). Therefore, the stacking sequence of the SiC biatom layers can define these polytypes.

3C-SiC is the only cubic crystal lattice structure of SiC form. There are only three possible available positions oriented for each SiC bilayer with regard to the lattice while it is maintained for the tetrahedral bonding. If the cubic crystal SiC structure has a stacking sequence with ABCABC, 3C-SiC is known as β-SiC, and the crystallographic structure would be cubic. Other non-cubic polytypes of SiC are known as α-SiC, except cubic polytype. Generally, β-SiC appears at relatively lower growth temperatures compared

to the other polytypes. In fact, relatively high temperatures are needed for the growth of 4H-SiC and 6H-SiC.

The polytypes of SiC are constructed by a stacking sequence of closely packed spheres; each sphere plane contains Si atoms, which is lying above the C atoms along the stacking axis denoted by the c-axis. Thus, the crystalline structure of SiC is characterized by different repetitions of stacking sequence of layers denoted as A, B and C. For example, if the bilayer's stacking sequence is ABAB..., then crystallographic structure is hexagonal and known as 2H-SiC. 4H-SiC has an equal number of hexagonal and cubic bonds, and the stacking sequence is ABCB. If the stacking sequence is ABCACB, it is referred to 6H-SiC consisting of one-third hexagonal bonds and two-thirds cubic bonds. Stacking sequences of Si-C bilayers and distinctions among four common polytypes of SiC are summarized in Table 2.1.

TABLE 2.1: Notations of four common different polytypes and corresponding inequivalent lattice sites.

SiC polytype	Stacking sequence	No. of hexagonal-like inequivalent sites	No. of cubic-like inequivalent sites
2H	AB	1	0
3C	ABC	0	1
4H	ABCB	1	1
6H	ABCACB	1	2

As discussed above, different stacking sequences of Si-C bilayers form different SiC polytypes. Every single Si-C bilayer can be regarded as a silicon atom connected with a carbon atom [19]. The schematic diagram of the stacking sequence of most familiar polytypes along the c-axis known as the stacking direction is showed in Figure 2.1.

SiC materials are very inert, impressively hard, and have high thermal conductivity. Properties like the impurity ionization energies, the saturated drift velocity, and the breakdown electric field strength are distinctive for the SiC polytypes. β-SiC exhibits the highest electron carrier mobility and the smallest bandgap compared to α-SiC, and it is a very significant SiC material widely used in the microelectronics industry. Due to these superior properties, SiC is an excellent material in the electronics industry applications such as the fields of high-temperature devices, high-frequency devices, high-power devices, and optoelectronic devices. Some specific examples include power switches, rectifiers, as well as microwave power devices [20]. In addition, SiC, which is reinforced

composite material and has high-temperature structure, can be also applied in the machine, car, aerospace, and petrochemical industries [21–23].

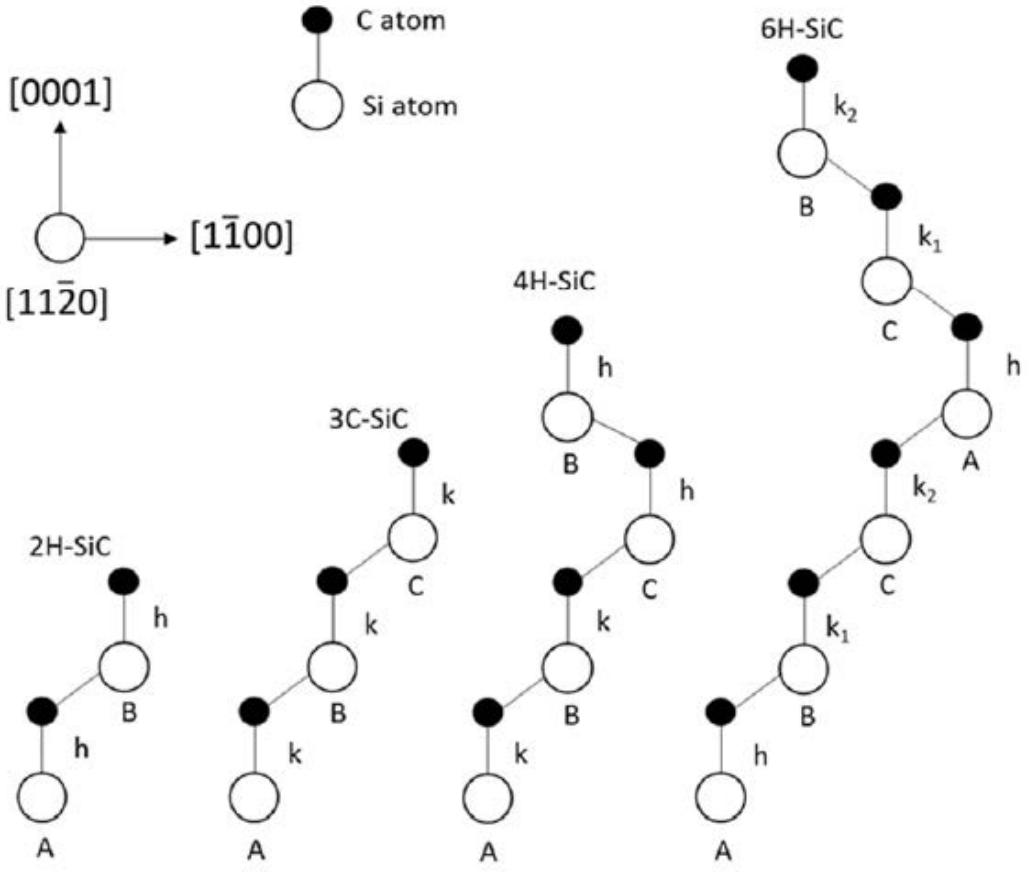

FIGURE 2.1: Stacking sequence of different polytypes of SiC. The cubic and hexagonal crystal symmetry points are represented by h and k respectively.

TABLE 2.2: Physical properties of SiC and other semiconductors.

Property	3C-SiC	4H-SiC	6H-SiC	Si
Melting Point (K)	3100	3100	3100	1690
Lattice Parameter (a, c in Å)	a=4.36 c=4.36	a=3.08 c=10.05	a=3.08 c=15.12	5.43
Bandgap (eV)	2.42	3.23	3.02	1.11
Saturation drift velocity (10^7cm/s)	2.5	2.0	2.0	1.0
Thermal conductivity (W/cmK)	5	5	5	1.5
Breakdown electric field (10^8 Vm^{-1})	1.5	3	3.2	0.6
Thermal expansion coefficient (10^{-6} /K)	3	-	4.5	2.6

Properties of several materials are different perpendicular to the c-axis or along the c-axis, because the hexagonal polytypes are composed of stacked double layers. Since the properties of material are directionally dependent, it is called anisotropy. Anisotropy of 1 is referred as isotropy and 3C-SiC is the only isotropic. The properties of the three common polytypes of SiC discussed above are shown in the Table 2.2 [24, 25] for comparison along with other commonly used semiconductor Si.

From Table 2.2, it can be shown that the breakdown electric field strength of SiC polytypes is almost 5 times higher than that of Si. This property of SiC makes it an excellent material for high power device applications, which can be operated at much higher voltages than that of Si.

2.2 Growth of SiC Nanowires

One-dimensinal SiC nanostructures have caught many scholars' attention due to their special mechanical, optical, and electronic properties. A remarkable progress in SiC nanowire growth methods have been accomplished by a variety of technologies, such as chemical vapor deposition using silicon precursor, conversion of carbon nanotubes and C-fibers, laser ablation, arc discharge, high-frequency induction heating, VS mechanism, VLS mechanism, and SLS mechanism, etc.

2.2.1 Chemical Vapor Deposition

Chemical vapor deposition methods are the most commonly used techniques for the synthesis of one-dimensional SiC nanostructures. Conventionally, 3C-SiC thin films are formed via chemical vapor deposition using precursors containing a silicon precursor (silane) and a hydrocarbon (methane, ethane, or propane). However, strict security control for using silane gas source is required for its toxicity, flammability, and explosive nature. Therfore, a single organosilane precursor like tetraethylsilane (TMS, $Si(CH_3)_4$) or hexamethyldisilane (HMDS, $Si_2(CH_3)_6$) has been employed in growing 3C-SiC thin films owing to its accurate stoichiometry, low growth temperature, safety, and ease of handling. Furthermore, low pressure chemical vapor deposition below 10 Torr is more favorable, because thin films with smooth morphology and uniformity would be grown during the 3C-SiC film growth process [26]. In the present paper, SiC nanowires were

successfully synthesized by low pressure chemical vapor deposition using HMDS as a precursor on SiO_2/Si substrate with various metallic catalysts, as shown in Figure 2.2.

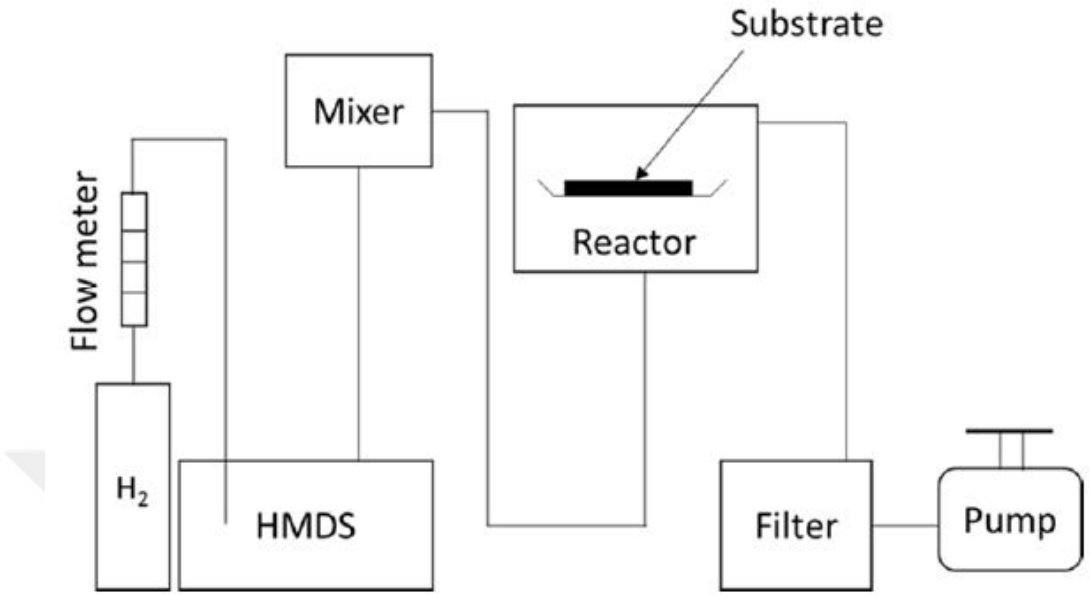

FIGURE 2.2: Schematic diagram of a chemical vapor deposition system.

HMDS is a colourless liquid metalorganic precursor, soluble in organic solvents. The rate of HMDS deposition is decreased with the increasing of growth temperature, which indicate that the photolysis of absorbed species on the substrate would be helpful for formation of the nanowires [27]. But HMDS decomposition reaction was stable in time. HMDS thermally decomposes at temperatures above 600 °C. In this study, HMDS decomposition has been shown to be first order forming $(CH_3)_3Si$ (trimethylsilane) radicals by breaking the silicon-silicon bond at temperatures below 1100 °C at first [28].

$$[CH_3]_3Si{-}Si[CH_3]_3 \longrightarrow 2\,(CH_3)_3Si$$

The possible unimolecular reaction series happened in the chamber results in the release of the methane (CH_4), acetylene (C_2H_2), and ethylene (C_2H_4) by extracting hydrogen from the $SiMe_3$ during decomposition of HMDS [29, 30]. The amount of the acetylene increases as the temperature of reactor increases, while the amounts of the methane and ethylene decrease when the reactor temperature is increased further.

$$[CH_3]_3Si + H \longrightarrow [CH_3]_2Si + CH_4$$

$$[CH_3]_2Si \longrightarrow C_2H_4 + SiH_2$$

$$[CH_3]_2Si \longrightarrow C_2H_2 + H_2 + SiH_2$$

A lot of methane is formed due to the sufficient hydrogen in the carrier gas. And acetylene and ethylene are formed at higher temperatures by unimolecular decomposition of the $[CH_3]_3Si$ radical [29]. Nevertheless, Si-Si bond in HMDS is very reactive in the environment where there is hydrogen [31]. So in hydrogen rich environment , the reaction of HMDS which is likely to happen at high temperatures may also lead to:

$$H + [CH_3]_3Si{-}Si[CH_3]_3 \longrightarrow [CH_3]_3SiH + [CH_3]_3Si$$

Then, due to the hydrogen in the carrier gas, SiC is formed by the reaction of carbosilanes [31].

$$H_2Si[CH_3]_2 + C_2H_4 \longrightarrow SiC + 3\,CH_4$$

The reaction results in the ralease of methane, but uses ethylene. The amount of methane decreases rapidly at temperature above 1000 °C. Chemical vapor deposition is a very useful and desirable growth method, which is widely applied to synthesis of SiC in different shapes of powders, nanorods, thin films, and whiskers with Si–C–H–Cl system [32–35]. It is known that high purity SiC nanowires were produced by a simple chemical vapor deposition growth method using metallic catalysts at normal atmosphere pressure.

2.2.2 Conversion of Carbon Nanotubes (CNTs) and C-Fibers

A variety of SiC nanowires growth experiments have been conducted using the reaction between CNTs and Si containing rich vapors that formed by the evaporation of solid SiI_2 or SiO [14], as seen in Figure 2.3. The reaction is as follows:

$$SiO(g) + 2\,CNT(s) \longrightarrow CO(g) + SiC(s)$$

The reaction begins on the outer surface of the nanotube towards the interior and gradually converts the CNTs into a SiC-based nanowire because of the segmented bamboo-like CNT structure, while there is no reaction going on inside the nanotubes [14].

Conversion of C-fibers has been also used for the formation of SiC nanowires. Electrospinning of polyacrylonitrile (PAN) nanofibers at ambient temperature and following carbonization at 700 °C would result in the producing of C-fibers. Then it is required to heat nano - fibers for one hour at 1600 °C under the atmosphere of Ar and SiO vapor [14]. SiO vapor, which was created through the silicon reduction of the silica, has a reaction with the carbon fibers to produce SiC nanorods. The reaction equations are as follows during the two-step reaction process:

$$\mathrm{Si(s)} + \mathrm{SiO_2(s)} \longrightarrow 2\,\mathrm{SiO(v)}$$

$$2\,\mathrm{C(s)} + \mathrm{SiO(v)} \longrightarrow \mathrm{CO(v)} + \mathrm{SiC(s)}$$

The benefit of C-fiber conversion process is that there would be a relatively large quantity of single-crystalline nanowires, and that these obtained nanowires have well-ordered structures, very low concentration of stacking faults, and uniform cross-sections. Compared to nanowires or SiC whiskers fabricated by the VLS mechanism, there is no containing catalyst during producing SiC nanowires s by the C-fiber conversion.

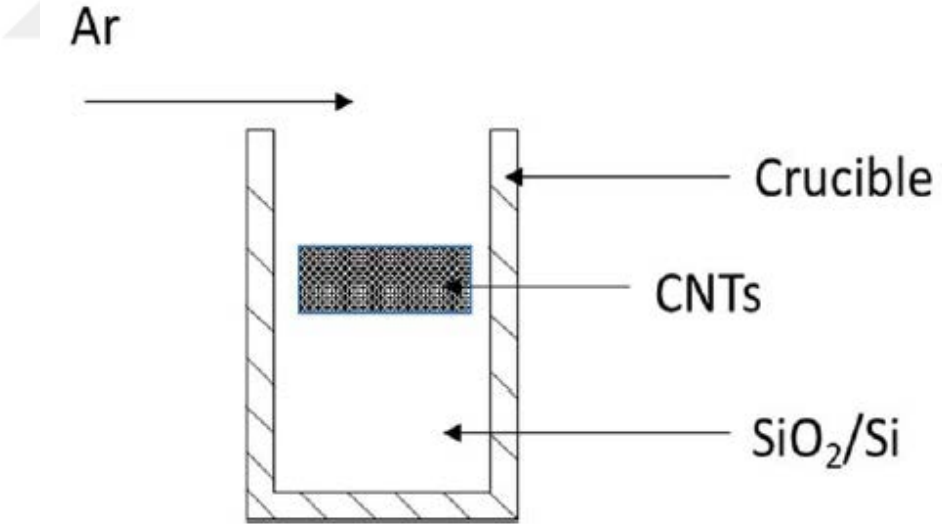

FIGURE 2.3: Geometry of the reactor of the conversion of CNTs and C-fibers.

2.2.3 Arc Discharge

It is a method that the nanowires were produced utilizing an arc discharge between two graphite electrodes. And the anode is made up by SiC rod. A graphite rod have a hole

drilled at one end and the other end is getting thinner. A SiC rod, which is plugged into the hole, used as the anode, then a graphite plate is used as the cathode, which is shown in Figure 2.4 [36].

A related growth process can be demonstrated as follows: During discharging, because of the high temperature of the arc-zone, SiC at the tip of the anode decomposes into carbon and silicon.

$$\mathrm{SiC(s)} \longrightarrow \mathrm{C(g)} + \mathrm{Si(g)}$$

There may be a reaction between silicon gas and the quartz (SiO_2) to produce SiO gas.

$$\mathrm{Si(g)} + \mathrm{SiO_2(s)} \longrightarrow \mathrm{SiO(g)}$$

Therefore, the absorption and dissolving of SiO, Si, and C gas in the liquid-iron droplets would leads to the formation of a liquid Fe-Si-C-O alloy. When it is cooled, the liquid droplets are supersaturated and the nucleation of β-SiC core along with the SiO_2 sheath is appeared [36].

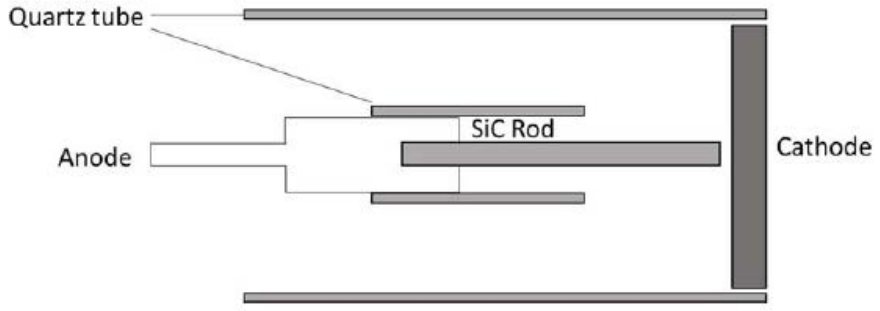

FIGURE 2.4: Arc-discharge setup.

2.2.4 Laser Ablation

Laser ablation has been widely used to form SiC nanowires and carbon nanotubes [37]. It is a method that can form high-purity nanoscale material at a relatively low operating temperature for multicomponent and high-melting materials [36, 37]. Laser-ablation technique, which is shown in Figure 2.5, was used to produce SiC nanowires from a SiC target. Laser beam focused on the SiC target was pulsed by the KrF excimer and the

ablation lasted for 2 hours. A great quantity of randomly oriented, curved, and straight nanowires were created on the graphite substrate in the system.

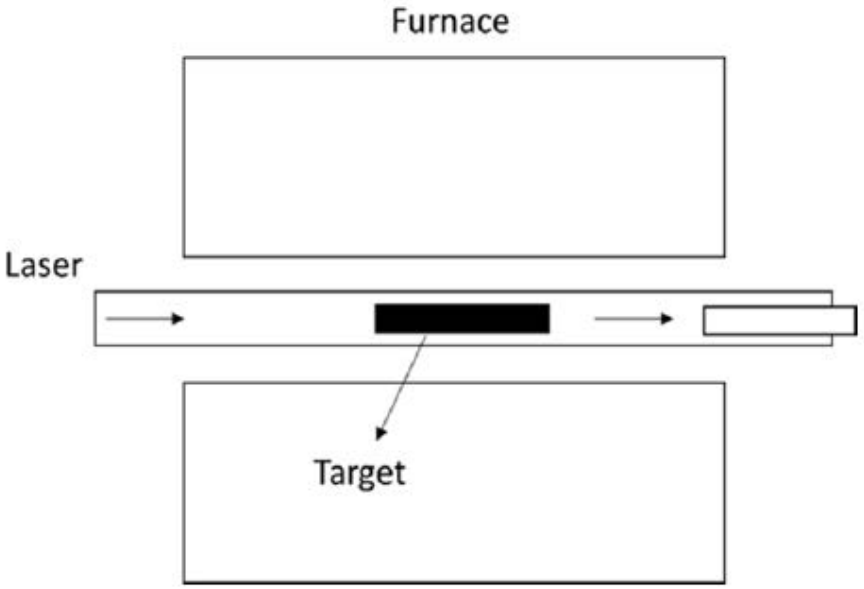

FIGURE 2.5: Laser-ablation.

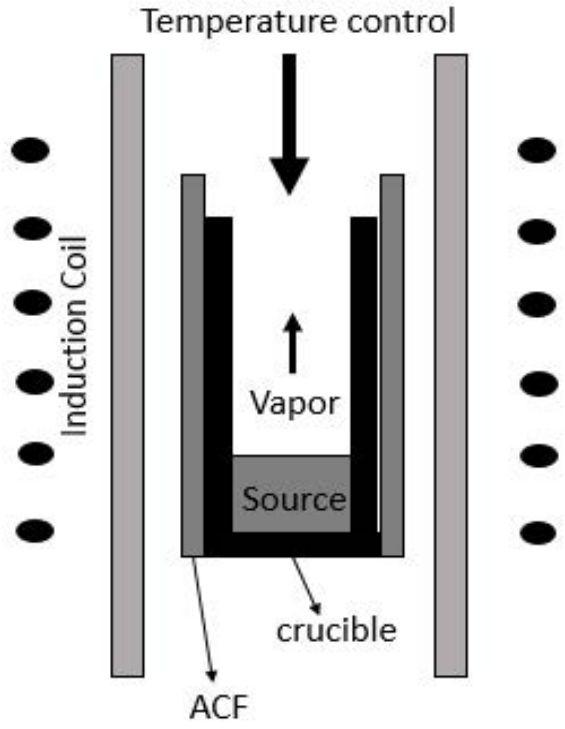

FIGURE 2.6: High-frequency induction-heating furnace.

2.2.5 High-Frequency Induction Heating

High-frequency induction heating is a unique process to produce SiC nanowires in high yields without using catalyst on the surface of the activated carbon fibers (ACFs).

As shown in Figure 2.6, the growth process is carried in a high-frequency induction-heating furnace, which includes an inductive heat cylinder of graphite covered by a quartz tube and a layer of ACFs. Nanowires synthesized by high-frequency induction heating are lots of mushroom shaped lumps, which grow separately and perpendicularly on the ACF surface and then connect each other at their tip. The procedure of the growth process represented by a flow chart is shown in Figure 2.6.

2.2.6 SiC Nanowires Growth Method Based on Vapor-Liquid-Solid Mechanism

The vapor-liquid-solid growth mechanism, which is shown in Figure 2.7, is the most common growth mechanism of SiC nanowires. In the VLS mechanism, V represents for vapor feed gases, L represents for liquid catalyst, and S represents for solid crystalline nanowires growth.

Different from all other nanowire growth methods, there is a liquid catalyst in the VLS mechanism. The catalyst forms a liquid solution interface along with the metal material, and it is grown from the vapor feed gases through the liquid-vapor interface. Feed gases from the vapor are deposited in the catalyst solution so that it results in supersaturation of the liquid [3]. At the solid-liquid interface, the supersaturated liquid is precipitated for the crystal growth.

In the VLS growth mechanism, first a vapor is rapidly adsorbed by a catalytic liquid alloy phase to supersaturation levels, and the subsequent crystal growth will occur at the liquid-solid interface from nucleated seeds. Nanoclusters are used for describing nucleation and succeeding growth process of nanowire. The advantage of catalyst used in VLS is the forming of the liquid phase occurring at low temperatures and the growth of a crystal in a high speed compared to the very slow crystal growth through a direct gas phase adsorption on to a solid surface. In VLS mechanism, the nanowires growth has the characteristic of systematic appearance of catalyst particles on their tips [14].

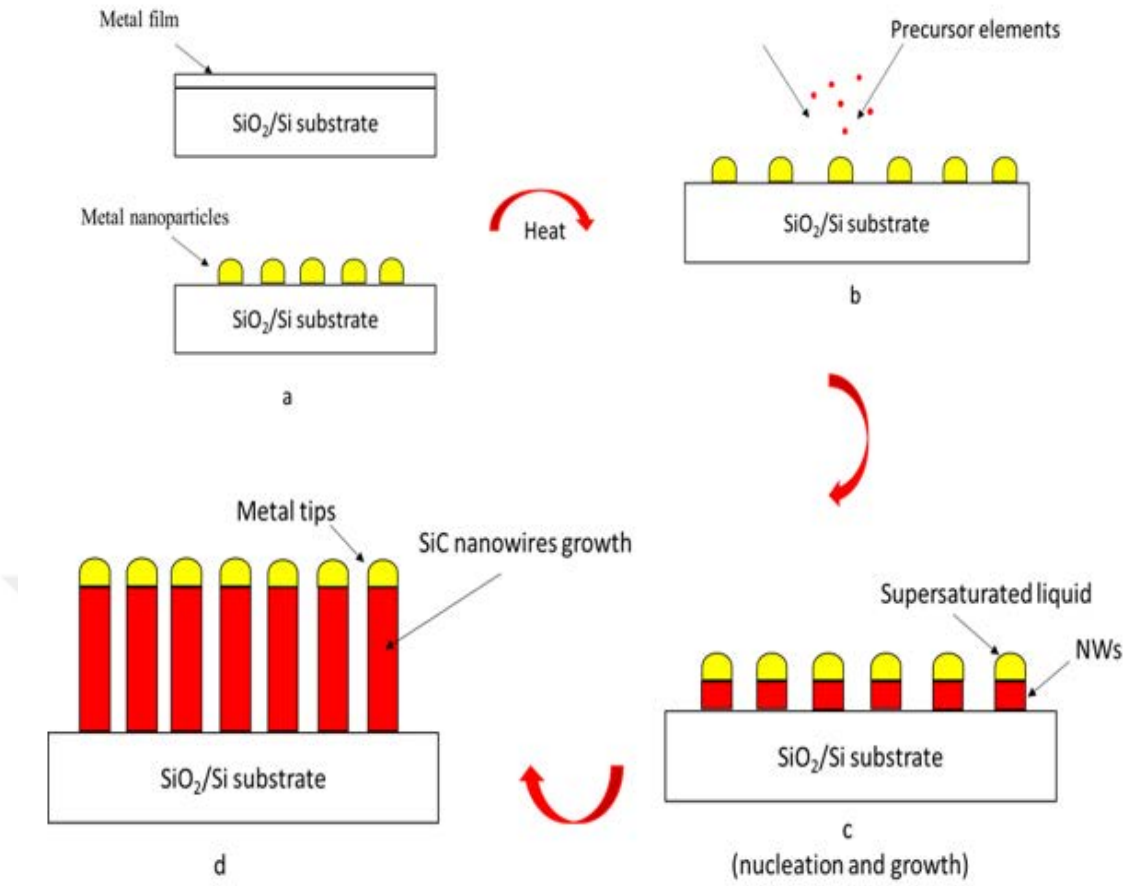

FIGURE 2.7: Schematic diagrams of VLS growth mechanism.

2.2.7 SiC Nanowires Growth Method Based on Vapor-Solid Mechanism

The vapor-solid mechanism of SiC nanowire growth process refers to the situation in which gaseous precursors with containing Si and C react on a solid surface to produce SiC nanowires. During the reaction, nanowires growth begins at nanometric nuclei formed in-situ and it goes on according one crystallographic direction. And this crystallographic direction is either feature of the thermodynamically favorable or crystal anisotropy. The nanometric nuclei are introduced by the forming of the nanoparticles with containing Si and C on the surface of the solid. Therefore, for the sake of fabricating nanosize nuclei for succeeding nanowire growth on top of the solid surface and to assure growth along one direction, an appropriate and well-controlled growth configuration has to be exploited. This VS mechanism of SiC nanowire growth with using Si and C gaseous precursors has been utilized without any appearance of a metallic catalyst.

For example, in the process of producing SiC nanowires, the VS mechanism experimental setup shown in Figure 2.8 is composed of an alumina boat holding polypropylene (PP) as well as a second alumina boat holding an equimolar blend of SiO_2 and Si, which is concealed by a graphite condensation plate. The whole VS mechanism setup system is put into the hot-zone of the alumina tube that is in a convective furnace. And the nanowires growth process continues few hours for forming radial heterostructures such as SiC/BN, SiC/SiO_2, and SiC/C by adjusting the precursor's concentration.

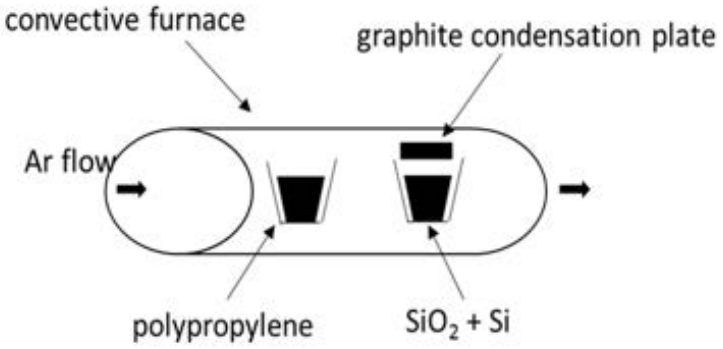

FIGURE 2.8: Vapor-solid mechanism setup.

2.2.8 SiC Nanowires Growth Method Based on Solid-Liquid-Solid Mechanism

The solid-liquid-solid mechanism growth method is a relatively simple methodology to produce SiC nanowires, because a gas phase precursor like $SiCl_4$, or SiH_4 is not required. During the entire process of the SLS mechanism, SiC nanowires can be directly formed on a single-crystal silicon substrate that performs the role of a silicon source without any presence of extra Si source from the outside. The carbon is supplied by deposition of a metal-rich catalyst-C thin layer such as Fe-C [38] and Ni-C [39, 40] on the silicon substrate. And the annealing of the catalyst deposited on Si substrate under Ar gas flow leads to the formation of the metal-silicon alloy nano-droplet. Consecutive silicon atoms diffusion from the substrate to the droplet at increased temperatures results in silicon atoms saturation inside the alloy droplet that causes silicon precipitation at the surface of the droplet. The Si precipitation on the surface produces a Si growth causing the formation of a thin layer nanowire on the surface of the substrate from the catalyst because of cooling down to room temperature at the droplet surface. Therefore, in most

cases SiC nanocables are fabricated with SiC nanowires as core and with a-C and SiO_X as sheath material.

Compared to the VLS mechanism, polytype phase and different orientation nanowires are produced by the SLS mechanism. Besides, SLS seems to be a useful process for forming SiC nanocables on the sheath material with a good control. In summary, SiC nanowires were controllably produced straightly on a Si substrate without any addition such as a liquid or gaseous Si source. Instead, the single-crystal silicon substrate forms silicon carbide nanowires acting as a source of Si.

2.3 Properties of SiC Nanowires

2.3.1 Field Emission

Due to the small curvature chemical inertness, tip radius, electrical conductivity, and high aspect ratio, wide-bandgap SiC semiconductors are encouraging materials for the development of next generation of large-area field-emission flat panel displays. SiC nanowires could be used in field-emission technology due to their exceptional field-emitting properties [41].

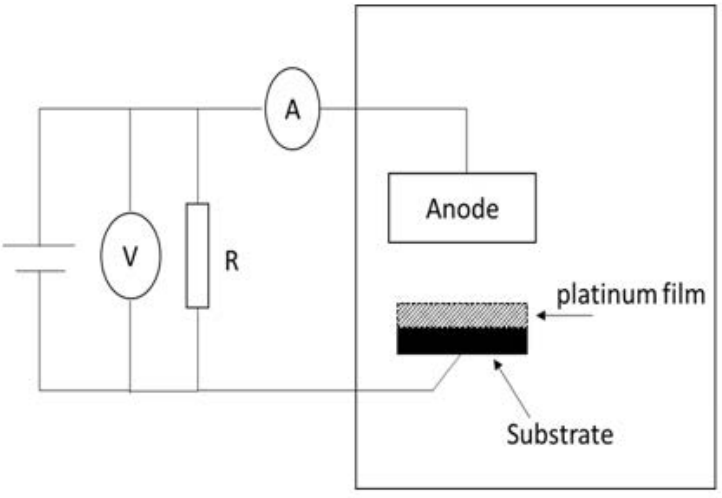

FIGURE 2.9: Experimental setup used for the field-emission measurement.

An experimental setup of the field-emission is shown in Figure 2.9. A stainless steel plate was used as an anode and a platinum film covered by glass substrate containing SiC nanowires was employed as a cathode. The distance (d) between the plate and

the emitting surface is decided by first lowering the plate to the product until electric contact is detected, and then picking the plate up to a required value [36]. The property of the field-emission is investigated by employing the first-order approximation of Fowler-Nordheim (FN) theory to know the emission features. The equation is as following:

$$J = \frac{1.56 \times 10^{-6} E^2}{\varphi} exp\big(- \frac{6.83 \times 10^{7} \varphi^{\frac{3}{2}}}{E}\big) \tag{2.1}$$

Where J is the field-emission current density (A. cm^{-2}), E refers to the microscopic local electric field at the emission sites (V. cm^{-1}), and φ represents for the work function of the emission tip (eV). The electric field (E) is measured by applied voltage V by determining $E = \beta$ V/d, where β is the field enhancement factor and d is the anode-sample separation. The FN emission properties can be investigated by the linearity of curves sketching ln (J/E^2) as a function of 1/E [36].

In general, SiC nanostructures are exhibiting excellent properties for the production of field emitters. As we know, a high aspect ratio is extremely preferable to achieve a low threshold voltage for emission in field emitter applications. With regard to SiC nanowires, in addition to a high aspect ratio, the low electron affinity is an another significant parameter, which allows the electrons emission for lower applied in electric fields and results in higher emission current density [14]. Furthermore, the desirable physical and chemical stability of SiC nanowires would lead to a longer lifespan for devices by reducing emission instabilities. Consequently, SiC nanowires are very favorable material for field emission applications.

2.3.2 Optical Properties

The optical properties of SiC nanowires have been investigated by utilizing different analytical techniques and optical characterization. For example, measurements of complex refractive index, which is significant parameter for materials selection for particular photonic applications, can determine the band gap and temperature variation of band gap of the nanowires [42]. Information relating carrier concentration, donor atom concentration, as well as plasmon frequency of nanowires can be achieved by analysis of the

infrared spectra of the nanowires. Metallic nanowires present interesting plasmon absorption effect. The energy of the surface plasmon band is affected by factors like particle shape, size, composition, inter particle interactions and surrounding media [42].

Figure 2.10 (a) shows photoluminescence (PL) spectra of SiC/SiO_2 nanocables produced by the low-cost arc-discharge method in deionized water [43]. It is shown that there are two broad PL peaks seating around at 317 and 368 nm on the SiC with 10 nm core diameter. However, SiC nanowires with 20 nm diameter keeps two emission peaks around at 312 and 393 nm. It is claimed the central SiC nanowire leads to the second peak and the blue shift may arise from the quantum size effects. Therefore, if the central SiC nanorod is thinner, then the corresponding PL peak energy would be higher [36].

Figure 2.10 (b) shows the PL spectra of the SiC with core diameter of 20 nm before and after annealing. It could be known that there is a little change in the positions of the PL peaks after annealing. It can be presented that local stress created during the SiC nanocables growth process would be released and there would be a decrease in quantity of surface-defects because of the high-temperature annealing, followed by the change in the PL peak's position and intensity. Therefore, the growth method and condition can obviously affect the optical properties of the SiC nanowires in terms of emission intensity and position, spectral shape and the existence of long wavelength components from defect states or impurity.

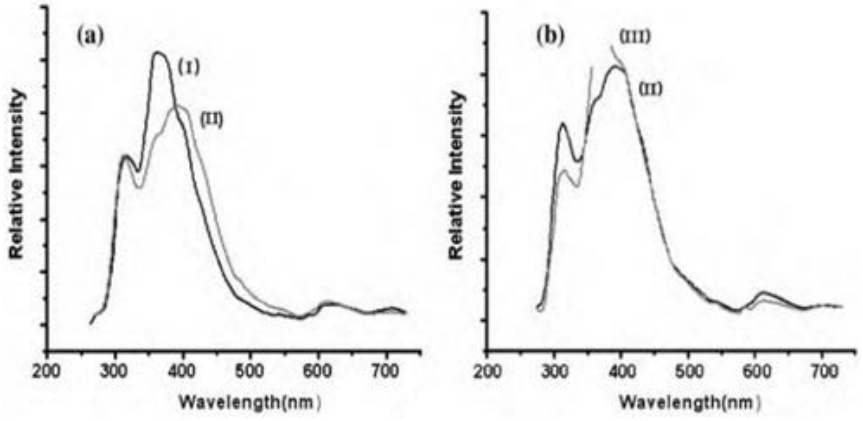

FIGURE 2.10: (a) PL spectra of the SiC nanocables (I) with core diameters of 10 nm and (II) with core diameters 20 nm, respectively. (b) The PL spectra of the SiC nanocables with core diameter of 20 nm (II) before annealing and (III) after annealing.

In summary, the PL spectroscopic research on semiconductor SiC nanowires have explained that there would be an increase in the band gap and PL energy peak with decreasing of the wire diameter. This phenomena prove the quantum confinement effect in nanowires as the wire diameter is decreased [42]. The fluorescence research of nanowires gives clear information related to the quantum confinement effect, band gap, electron effective masses, oxygen vacancies, and strain in nanowires. Magneto optic techniques can measure the amount of subbands of the nanowires. And it is very significant for establishing the electron transport properties of nanowires if the number of subbands in nanowires is determined [42].

Besides, remarkable optical properties and uniform morphology of SiC nanowires have caused their latent capacity for their variety of optical applications. The nanowires' n-p junction has been expected for light emission, as a result of their electroluminescence or PL properties. The p-n junction of SiC nanowires has been considered to be used for laser applications. Non-linear optical properties of nanowires, which are exhibited by nanowire arrays, make them very desirable for photonic material application. The reducing of the wire diameter as well as the dramatic increasing of the energy of the absorption peak leads to the appearance of the blue shift and quantum confinement effect [42].

2.3.3 Electron Transport Properties

Electron transport properties of SiC nanowires are very significant for studying the distinctive one-dimensional carrier transport mechanism as well as electronic and electrical applications [42]. It has been known that the important parameters such as quality and crystal structure, chemical composition, wire diameter, wire surface condition, crystallographic orientation along with the wire axis affect the electron carrier transport mechanism of nanowires. Nanowires have practical potential in various electronic applications such as nanowire field effect transistors. The field-effect transistor, which is a transistor, controls the conductivity of the charge carrier by using an electric field.

The one-dimensional nanowires perform both diffusive and ballistic type electron transport mechanism that is determined the diameter and wire length. Ballistic type transport mechanism is related to the carrier flow without scattering, because the carrier mean free

path is longer compared to the mean free path of the wire length [42]. Ballistic type transport mechanism is examined at the connection of nanowire and other external circuits [44, 45]. At this contact junction, the conductance is quantized into an integral multiple of $2e^2/h$ (h is the Plank's constant and e is the electronic charge) [46, 47].

Figure 2.11 (a) shows a typical I_{ds}-V_{ds} feature of field-effect transistors of the SiC. It is shown that with the increasing of the gate voltage Vg, the conductance increases, which corresponds to the following formula:

$$\mu_e = \frac{g_m L^2}{C V_{ds}} \tag{2.2}$$

Where g_m is transconductance calculated as $g_m = dI_{ds}/dV_g$ and the gate capacitance C is estimated by

$$C = \frac{2\pi\varepsilon\varepsilon_0 L}{\ln\left(\frac{2h}{r}\right)} \tag{2.3}$$

Where r, h, and ε represent the radius of the SiC nanowire, the thickness of silicon dioxide, and the dielectric constant, respectively.

I_{ds}-V_{ds} curves achieved under the different temperatures at Vg = 5V of the n type SiC nanowire field-effect transistor [36] is shown in Figure 2.11 (b).

It can be presented that there would be one order of magnitude increase in the drain current with decreasing of the temperature from the room temperature. It is generally considered that the gate voltage Vg influences the R_{SiC} value via modulation of the Fermi level, thus the slope is changed. The liner relation, as shown in the Figure 2.11 (b) (low-right inset), describes as an Arhenius function:

$$\mu_e = \mu_0 exp\big(-\frac{E_a}{KT}\big) \tag{2.4}$$

Where μ_0 is the pre-exponential factor, Ea refers to the activation energy, and k represents for the Boltzmann constant. It can be shown that with the increasing temperature, the carrier mobility would be increased.

Get to knowing the thermal transport in nanoscale and then producing nanoscale materials with very high or very low thermal conductivities have an effect on electronic devices and also contribute to the design of new thermoelectric materials [14]. For example, heat dissipation is significant for highly integrated devices and nanodevices could be considered to be used for high integration applications. The wire diameter of nanowires affects its thermal conductivity. The enhanced thermo power and increase of the seebeck coefficient of nanowires would be very beneficial for energy conversion devices and thermoelectric cooling system.

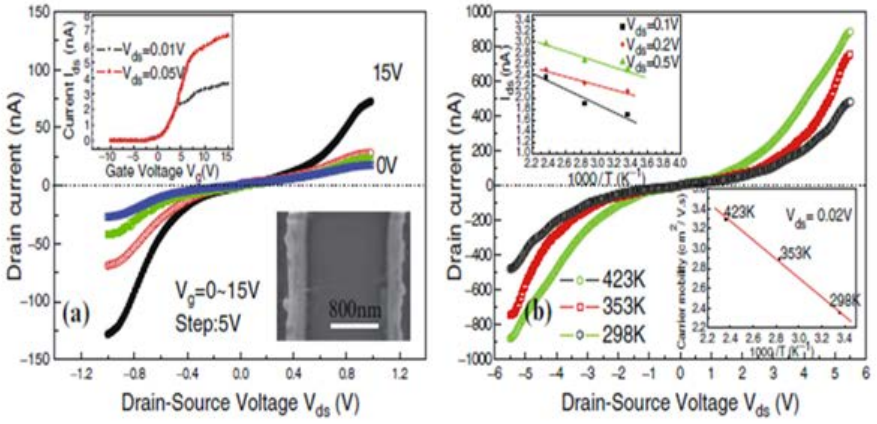

FIGURE 2.11: (a) Current (I_{ds}) versus voltage (V_{ds}) curves at different gate voltages. (b) I_{ds} versus V_{ds} curves obtained at the different temperatures at Vg = 5V.

2.3.4 Mechanical Properties

One-dimensional nanostructure-based materials are stronger than their counterparts. SiC nanowires would play the role of reinforcement of materials for ceramic matrix composites to make a progress in their strength and toughness [48, 49]. Figure 2.12 shows a typical flexural stress versus displacement curve [36].

From the Figure 2.12, it can be seen that the T-NFRC composite (NFRC represents SiC nanowire/fiber-reinforced composites and T represents Tyranno-SA fiber) exhibits common characteristic with conventional Tyranno-SA/SiC composites (TC50, T-C100, and T-C200) for flexural fracture. Nevertheless, Tyranno-SA/SiC composites reinforced by SiC nanowire represent noticeable developments on the work of fracture and flexural strength compared to the conventional Tyranno-SA/SiC composites (T-C50, T-C100, and T-C200).

In a study [50], an extremely big strain plasticity, which is the capability of a material showing an unusually higher deformation rate during the SiC nanowires mechanical deformation process, has been investigated by a high-resolution transmission electron microscopy technique at temperatures approaching room temperature. It was found that there was a reduction of the dimensionality because of the increasing dislocation density at the beginning stage, and then occurring a distinct lattice deformation, and finally gets a total structure amorphization at the most strained region of the nanowires.

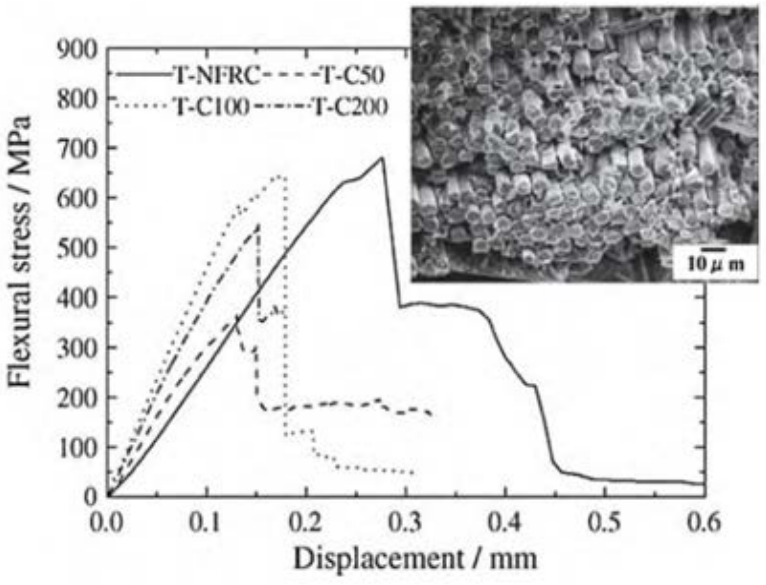

FIGURE 2.12: Flexural stress versus displacement curves and fiber pullout fracture surface (T-NFRC).

2.3.5 Photocatalyst Properties

It is widely known the photocatalytic activity of a semiconductor material is intensely affected by the surface area of the material. The photocatalytic reactions with higher efficiency depend on the large surface area of the nanosized material.

The photocatalytic activity of the SiC nanowires is analyzed by evaluating the photo degradation rates of acetaldehyde (CH_3CHO) for SiC in as a function of ultraviolet irradiation time under the ultraviolet light [51, 52]. It was known that a reinforced conversion of acetaldehyde with gaseous state is affected by the increase in the initial gaseous acetaldehyde concentration. This is because of the great number of gaseous acetaldehyde molecules, which are on the surface of the SiC nanowire powders [52]. It

was shown that the wonderful photocatalytic activity results in the effective acetaldehyde decomposition by ultraviolet light irradiation.

Chapter 3

Experimental Details

3.1 Nanowire Growth Setup and Procedures

SiC nanowires were synthesized by chemical vapor deposition on Si and SiO_2/Si substrate using HMDS as a precursor at temperatures between 900 and 1100 °C under carrier gas H_2. A conventional resistance heated hot-wall 25-mm horizontal low pressure chemical vapor deposition reactor was used to grow SiC nanowires, as shown Figure 3.1. Various catalyst materials, such as iron film, nickel film, and cobalt nanoparticles have been used.

High density of SiC nanowires have been produced at even lower temperatures of 900 °C in spite of the lower efficiency of source decomposition. The diameters range of SiC nanowire are between 8 nm and 60 nm. For the nanowires grown on Si substrate, the substrate was firstly ultrasonically washed in isopropyl alcohol, acetone, and de-ionized water and then dried in the nitrogen gas. Nanoparticle solution was utilized to the surface of the substrate and then dried. A quartz boat holding the Si and SiO_2/Si substrate was put into the chemical vapor deposition reactor. Then, the chemical vapor deposition reactor was evacuated and purged three times with hydrogen (99.999 %) [53]. After purging cycles, when the growth temperature is reached (typically between 900 and 1100 °C), HMDS was introduced to the reactor for typically about 15 min. HMDS ($Si_2(CH_3)_6$) is a liquid metalorganic precursor. The flow rates of HMDS and H_2 gas were controlled by mass flow controllers and set to 5 sccm and 500 sccm, respectively. After the growth, the supply of HMDS precursor was stopped and the reactor was cooled down

to the temperature of 250 °C under carrier gas H_2. Finally, the furnace was cooled down to the room temperature.

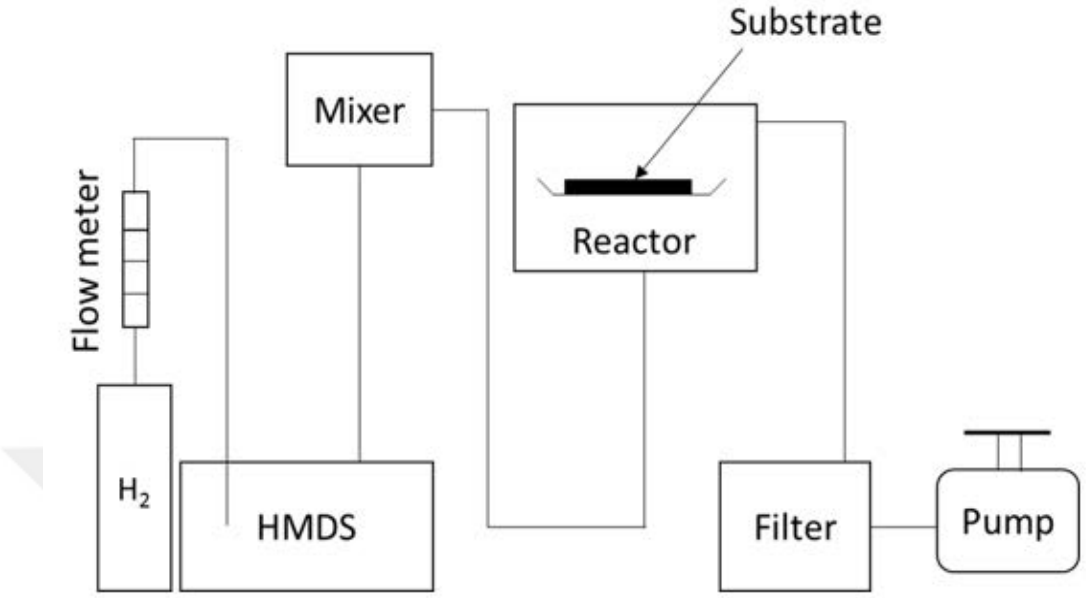

FIGURE 3.1: Schematic diagram of experimental set up for the growth of SiC nanowires.

3.2 X-ray Diffraction

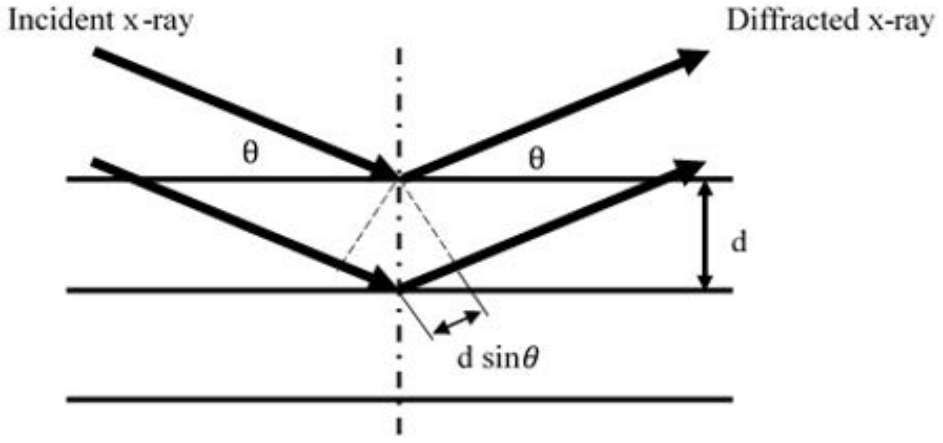

FIGURE 3.2: Schematic diagram showing the principle of XRD.

X-ray diffraction is a very valuable tool to investigate the physical properties, chemical composition, and crystallographic structure of nanomaterials. It can also be used to measure a variety of structural features of crystalline phases such as grain size, defect structure, strain, and phase composition. XRD is also a beneficial method to establish the

organization of atoms within a crystal, which can be either polycrystalline structure or single crystalline. An X-ray beam strikes into a crystal and diffracts into many particular directions (see Figure 3.2).

From the XRD, we can decide the chemical bonding, disordering, and the crystal structure of the materials. Besides, it is a non-destructive method which precisely reveals information concerning unit cell dimension, crystalline structure and phase identification of materials. The structural properties of the nanowires were characterized by a Bruker D8 Discover with K_α radiation of copper (Cu) at wavelength of 1.54 Å [54].

The XRD works when there is a parallel monochromatic x-ray beam hitting on a sample, part of the beam will be diffracted by different crystal planes of the sample. The diffracted rays will interfere with each other to form diffraction spots and form constructive interferences in certain angles. These constructive diffraction interferences of the sample should obey the Bragg's Law:

$$2d_{hkl}\sin\theta = n\lambda \tag{3.1}$$

Where d_{hlk} is the inter-planar spacing, θ refers to the angle of diffracted beam, n refers to an integer that represents the number of diffraction mode, and λ is the wavelength of the incident x-ray beam.

The angle between the diffracted and transmitted beams will be equivalent to 2θ all the time. Therefore, the results of XRD are expressed in terms of 2θ, and this angle can be obtained easily in experimental conditions. For a material with a cubic structure, the inter-planar spacing can be deduced from the equation:

$$d_{hkl} = \frac{a}{\sqrt{h^2+k^2+l^2}} \tag{3.2}$$

Where k, h, and l are the Miller indices.

But for hexagonal structure, the formula should be the following:

$$\frac{1}{d_{hkl}} = \sqrt{\frac{4}{3}\left(\frac{h^2+k^2+l^2}{a^2}\right)+\frac{l^2}{c^2}} \tag{3.3}$$

Where k, h, and l are the Miller indices.

Two different scanning modes, θ-2θ mode and rocking mode, were employed to characterize the crystal structure of the SiC nanowire. The first mode is to identify the crystalline phases and orientation of the film. In this mode, the x-ray source is fixed, and the sample holder is moving in the speed of ω and the detector is moving in the speed 2ω. The second mode is the crystalline structure measurement of the sample by deciding the FWHM from the rocking peak. this mode, The X-ray source and detector are fixed at a selected angle, where the sample holder is rocked back and forth in a few degrees about the θ direction so as to determine the crystallinity of the sample from the FWHM in the rocking curve [55].

3.3 Scanning Electron Microscopy

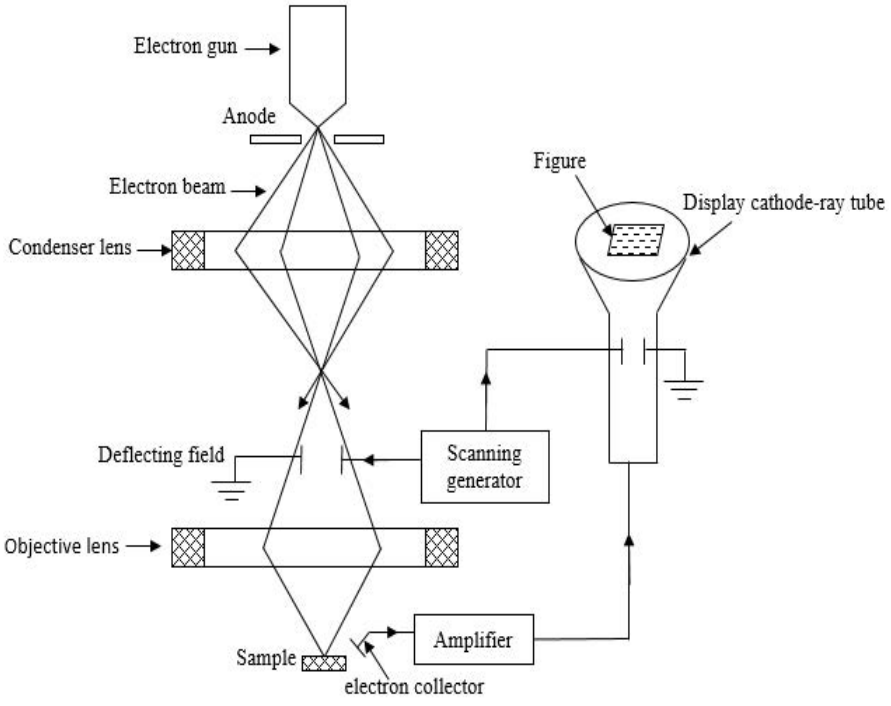

FIGURE 3.3: Scheme of scanning electron microscope.

Scanning electron microscopy is a high resolution electron microscope capable of imaging the surface of the sample by scanning it with high-energy beam of electrons generated from an electron gun [56], (see Figure 3.3). The sample's composition, surface topography, as well as other kinds of properties like electrical conductivity can be obtained when the electrons from the electron gun interact with atoms from the sample, which is

shown in Figure 3.4. Both electron and photon signals are launched, when the sample is struck by the electron beam. Typically, there are several types of signals produced by SEM, including characteristic x-ray, back-scattered electrons, cathodoluminescence, transmitted electrons, and secondary electrons, which are shown in Figure 3.4.

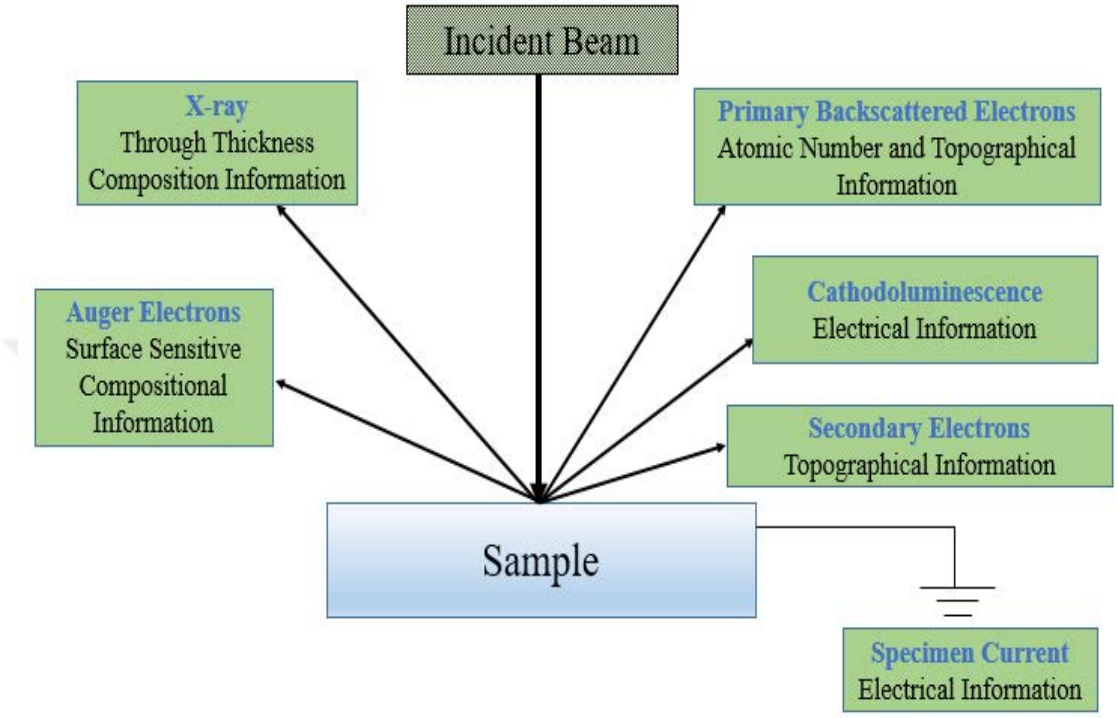

FIGURE 3.4: Schematic diagram showing the principle of scanning electron microscopy.

Secondary electrons emitted by the sample surface are electrons in the sample that are emitted by the beam electron. It does not take much energy for ejecting the electrons that is in the valence bands or conduction, and these electrons are known as slow secondary electrons with energies below about 50 eV. The electrons in strongly bound inner-shell are not easy to be ejected readily. However, they can have an important part of the beam energy when they are thrown out of their shells, so called fast secondary electrons. When an ionized atom returns to the ground state, the secondary electrons ejected by the released energy from an inner shell are called Auger electrons.

Back-scattered electrons and secondary electrons and are the most commonly imaged signals in SEM. Secondary electrons are the essential imaging signal in SEM in which they provide high topographic sensitivity and good spatial resolution. Secondary electrons are electrons from specimen atoms, which have been ejected by beam electrons. It is possible for the secondary electrons to be escaped from the subject sample if the

electrons are very close to the surface, and they also have very low energies. This gives secondary electron images strong topographic contrast and high spatial resolution. The back-scattered electrons signal mainly gives information about its strong atomic number contrast. Elastically scattered beam electrons, which have been directed and returned from the sample surface, consist of the backscattered electron signal.

Electrons bombarding the sample result in the emission of X-rays whose energy is feature of the sample's elemental composition. Besides, X-rays are also extensively applied for elemental microanalysis. The dispersive x-ray spectrometer can be used to count and classify x-rays' characteristic on the basis of their energy. The quantitative elemental composition of the specimen is able to be calculated by the intensity of the x-ray signal at each energy spectrum.

3.4 Transmission Electron Microscopy

Transmission electron microscopy is a high resolution microscopy, having higher resolution than SEM, which depends on electron beam ejected from an electron gun to transmit through an ultra-thin sample. The electron beam will be diffracted as it passes through the sample so that a diffraction image and crystalline structure image can be formed, which can be measured by a charge-coupled device sensor, (see Figure 3.5). A TEM has four main elements such as a control software, an electron optical column, the necessary electronics, and a vacuum system [55].

The electron optical column contains elements that have the same features with those of a light microscope. An electron gun that is put into the column, is replaced for the light source of the light microscope. At first, the electron beam emitted from the electron gun becomes almost parallel beam condensation on the sample surface by the condenser lenses. And then transmitted electrons are gathered and focused by the objective lens after passing through the sample. Finally, on the viewing device at the bottom of the column, a magnified image of the sample projected by the projection lens is appeared. The whole electron path process from gun to camera should be conducted in a vacuum system [55].

Initially, TEMs employed a film camera to record high resolution images and a fluorescent screen for real-time imaging and adjustments. This fluorescent screen emitted light

as it was hit by the transmitted electrons [55]. However, the screen that was in the projection chamber under vacuum system could be examined across a window by utilizing a binocular magnifier if it was needed. For capturing images of the specimen, modern instruments depend on solid-state imaging devices like the charge-coupled device camera.

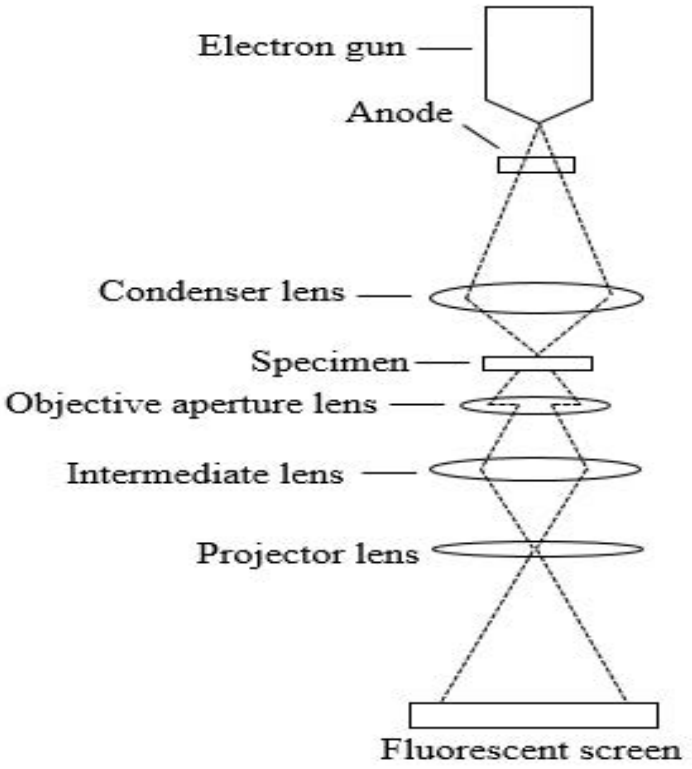

FIGURE 3.5: Scheme of transmission electron microscope.

During the nanowires examination, the acceleration of the current and voltage through the lenses is supposed to be highly stable to get a very high resolution. The power supply cabinet supplies a certain amount of power whose output current or voltage does not deviate, and very complicated electronic circuits are needed for such stabilizations.

Electrons act like light only when they are operated in vacuum system. As the same as discussed above, the entire system from the source to fluorescent screen is needed to be evacuated. A variety of vacuum levels are needed during the process: the highest vacuum is found on the source material and the specimen, a lower vacuum is placed in the camera chamber and projection chamber. For obtaining and maintaining and these vacuum levels, different vacuum pumps are needed. A specimen or a filament or photographic material is interchanged, a lot of separation valves and airlocks are built in to avoid having the evacuation of the whole column at each time. The vacuum system is

entirely automated and the vacuum level is well protected against operational error and incessantly monitored in modern TEMs.

A TEM can be utilized to investigate the internal microstructure of samples down to the atomic level in any science and technology field. It is essential to make the sample thin enough to allow the transmission of electrons and small, stable enough to admit its introduction into the evacuated microscope system. Different applications require different thicknesses of materials. For example, the sample cannot be thicker than 20 nm for the ultimate high resolution materials investigations, but the film can be 300-500 nm thick for bio-research studies. Thus for the electron microscopy investigation of materials, each branch of scientific research study has its own unique particular methods for the preparation of the specimen.

3.5 Fourier Transform Infrared Spectroscopy

Infrared spectroscopy deals with matter electromagnetic field interacting in the infrared radiation (IR) region as a function of photon frequency. The Figure 3.6 shows the schematic diagram of FTIR for detailed analysis process of the sample which is exposed to the infrared radiation. Firstly, a glowing black-body light source emits infrared energy beam. Then the infrared beam enters the interferometer where the interferogram signal creates. After then, the beam enters the sample compartment where it is transmitted through or reflected off of the surface of the sample. When materials are exposed to infrared radiation, molecules of the sample absorb radiation of definite wavelengths that results in the change of dipole moment of molecules. Some of the infrared radiation is transmitted by the sample and some of it is absorbed. As a consequence, the vibrational energy levels of the sample molecules transfer from the ground state to the excited state. The resulting spectrum demonstrates the transmission and absorption of the sample molecules, and creates the sample's molecular fingerprint. The absorption peak frequency determines the vibrational energy gap of sample molecules and the number of the absorption peak is corresponding to the number of molecule's vibrational freedom. The magnitude of absorption peak is determined by the possibility of the transition of energy levels and the change of dipole moment. Finally the infrared beam enters to the detector for final measurement. The measured signal is digitized and sent to the

computer for the Fourier transformation. The final infrared spectrum is then presented to the user for interpretation and any further manipulation.

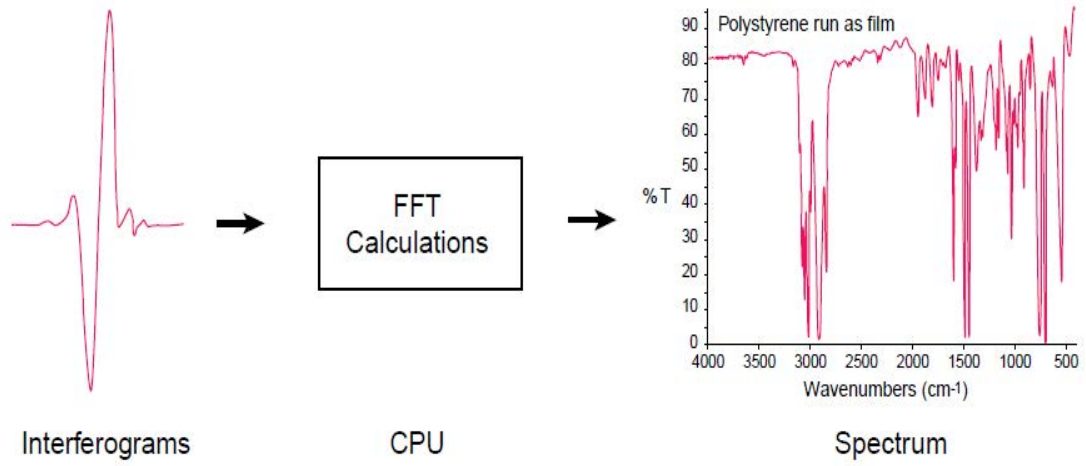

FIGURE 3.6: Schematic diagram of FTIR for analysis process of the sample.

The mathematical expression of Fourier transform can be presented as

$$F(\omega) = \int_{-\infty}^{+\infty} f(x) e^{i\omega x} dx \tag{3.4}$$

And the reverse Fourier transform is

$$f(x) = \frac{1}{2\pi} \int_{-\infty}^{+\infty} F(\omega) e^{-i\omega x} d\omega \tag{3.5}$$

Where ω refers to angular frequency and x refers to the optical path difference. F (ω) means the spectrum and f(x) is named as the interferogram. It is known that if the interferogram f(x), is determined experimentally, the spectrum F (ω) can be obtained by using Fourier transform. The relationship between the interferogram and the spectrum will be explained more fully in the latter sections.

FTIR gives valuable information about the rotation and vibration of the molecular structures and chemical bonding status of the materials, which make it easier for investigating both inorganic and organic materials. Besides, an infrared spectrum provides information about a sample's fingerprint with absorption peaks associated with the vibrations frequencies between the bonds of the sample atoms. Since each unique composition of atoms makes up different materials, there are no two materials creating the exact same

infrared spectrum. Consequently, infrared spectroscopy can lead to an identification of materials. Besides, with the FTIR, we are able to decide the quality of a sample, identify unknown materials and the components amount in a mixture.

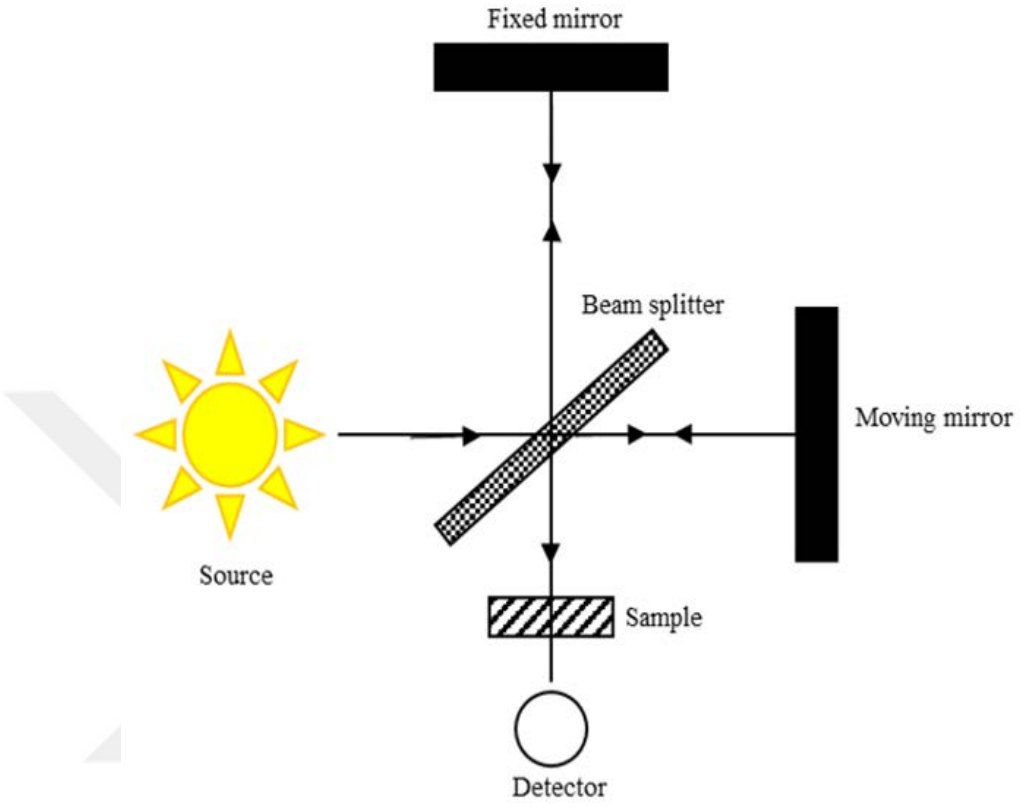

FIGURE 3.7: Schematic diagram of Michelson interferometer.

In an FTIR system, there are three basic spectrometer parts, which are a radiation source, an interferometer, and a detector. Firstly, interferometer creates an optical path difference between the radiant beams by dividing it, and then produce repetitive interference signals by recombining radiant beams. Interference signals are measured as a function of optical path difference by a detector. After passing through a sample, interference signals produced by the interferometer provide infrared spectral information. Michelson interferometer is one of the most commonly used interferometers. It includes active components: a fixed mirror, a moving mirror, and a beam splitter, which are shown Figure 3.7.

The moving mirror is perpendicular to another fixed mirror. The beam splitter is a semi-reflecting device and it is made by putting a thin film of germanium onto a flat KBr substrate. Broadband IR source generates radiation, which goes into the interferometer in a collimated way, and impinges on the beam splitter.

In a homogeneous medium, the absorbance of a single compound at any frequency is presented as,

$$A = abc \tag{3.6}$$

Where A refers to the measured sample absorbance at the given frequency, a represents for the molecular absorptivity at the given frequency, b means the path length of source beam in the sample, and the concentration of the sample is denoted as c [57]. It is indicated that there is a linear proportional between the concentration of every component in a solution or homogeneous mixture and the intensities of absorption bands by this law.

Generally, the most significant benefits of FTIR spectrometers are that the signal-to-noise ratios for a spectrum is high for the same measurement time and there is an improvement in spectra frequency measurement. Both the simultaneous measurement of the high optical throughput of the FTIR spectrometer and of detector signal for all the resolution of the spectrum result in the improvement of the signal-to-noise ratio.

Applications of FTIR spectrometers are widely used in industry [58], research [59, 60], and medical science [61]. FTIR can provide important information about both frequency and time domains in industrial applications. Hence, a large quantity of data can be investigated with high-accuracy in a very short time. In recent years, spectra of a very small sample of material is allowed to be obtained rapidly with preparation of the little sample by microbeam FTIR spectrometers, which is economically significant, because it leads to more data for materials at a lower cost. Besides, FTIR can also be used to determine the chemical characteristics of organic contamination in the semiconductor, and in biomedical and disk drive industries. FTIR spectroscopy, which can be employed as a nondestructive and rapid useful technique to determine the constituents of various materials.

Chapter 4

Structural Characterization of SiC Nanowires

SiC nanowires were practically synthesized by low pressure chemical vapor deposition process using HMDS as a precursor on SiO_2/Si substrate with various metallic catalyst such as iron film, nickel film, and cobalt nanoparticles. SiC nanowires were grown by a conventional resistance heated hot-wall 25-mm horizontal low pressure chemical vapor deposition reactor at temperatures ranging form 900 to 1100 °C under H_2 as both carrier and source dilution gas at atmospheric pressure. Fe-film and Ni-film were pre-deposited on SiO_2/Si and Si substrate by sputtering, respectively. Cobalt nanoparticle solution was applied to the Si substrate by micropipette. The HMDS and H_2 gas flow rates were controlled by mass flow controllers and set to 5 and 500 standard cubic centimetres per minute (sccm), respectively.

The samples have been characterized by scanning electron microscopy, x-ray diffraction (Rigaku 300), transmission electron microscopy, and Fourier transform infrared spectroscopy (FTS 7000 Series DigiLab with UMA 600 microscope) [53].

4.1 Structural Characterization

Figure 4.1, Figure 4.2, and Figure 4.3 exhibits SEM images of dense SiC nanowires synthesized at 1100 °C using Fe-film, Ni-film, and Co nanoparticles on SiO_2/Si and Si substrates. The SEM images show that large number of SiC nanowires with high aspect

ratios have successfully been synthesized with different catalysts materials. Majority of SiC nanowires grown with Fe and Ni-film catalysts are straight, while the majority of the nanowires grown with Co nanoparticles are curved.

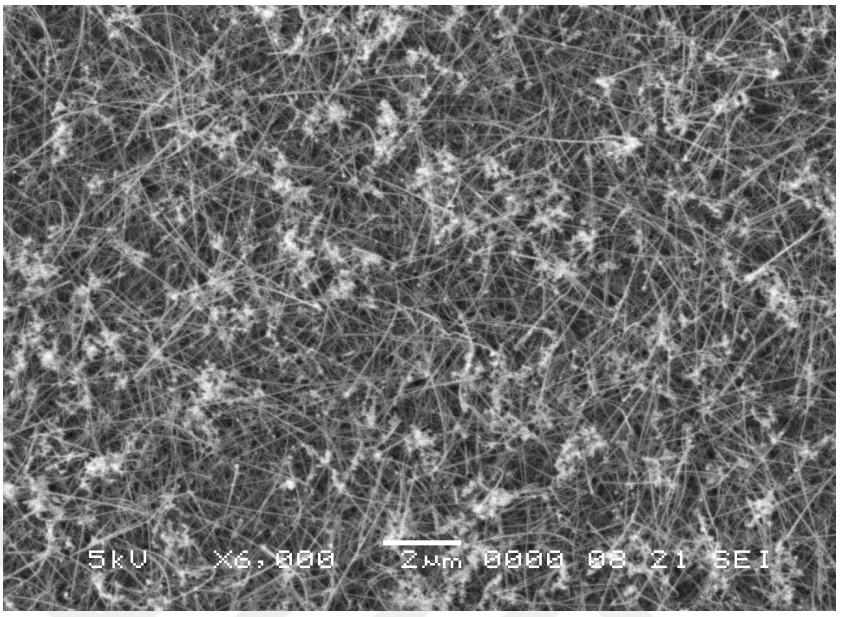

FIGURE 4.1: SEM images of high density SiC nanowires grown at 1100 °C with catalyst Fe-film.

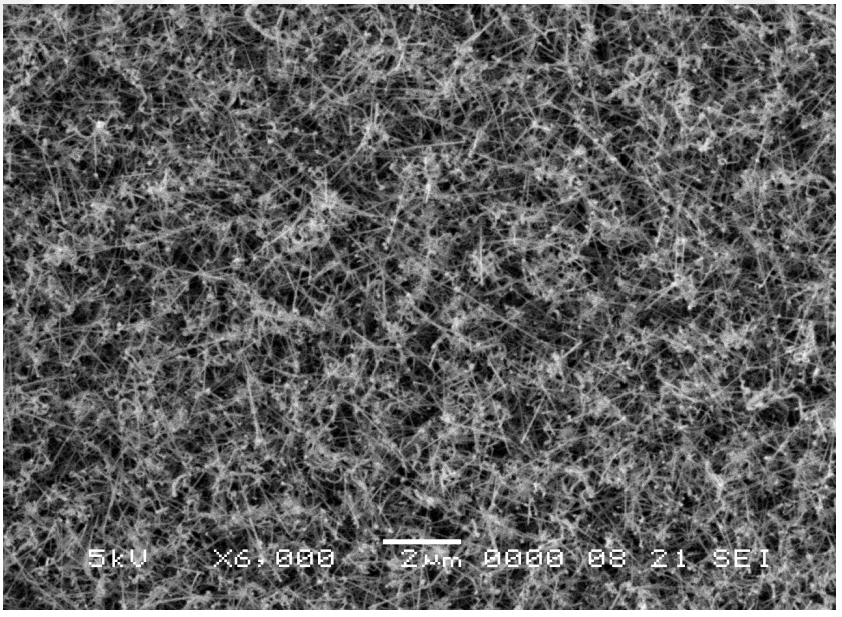

FIGURE 4.2: SEM images of high density SiC nanowires grown at 1100 °C with catalyst Ni-film.

Nanowires are very long with mostly lengths of several tens of microns. The diameters of the SiC nanowire grown with Fe and Ni film catalyst are about 30 nm (mostly), whereas the SiC nanowire diameters grown with Co nanoparticles occasionally reach to

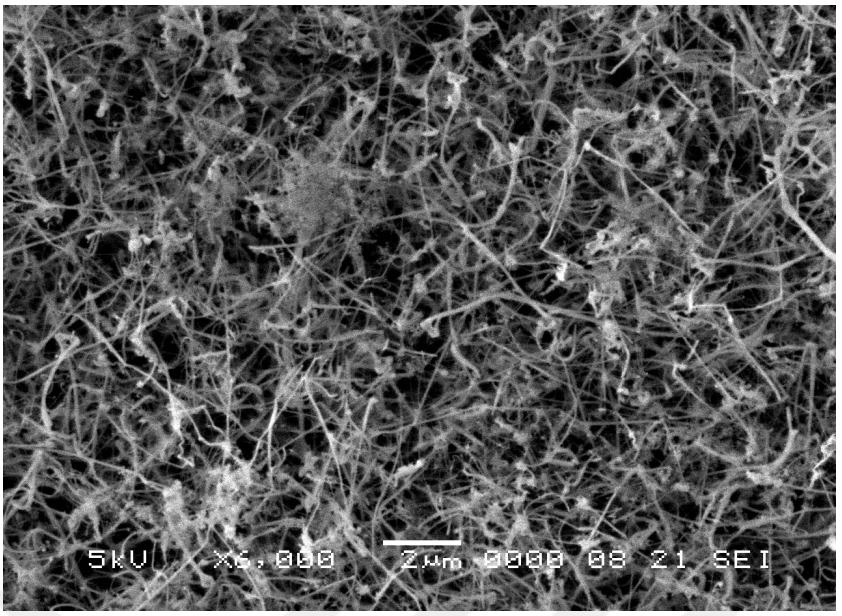

FIGURE 4.3: SEM images of high density SiC nanowires grown at 1100 °C with catalyst Co nanoparticles.

90 nm. The metal catalysts were seen at the end of the nanowires, which illustrate that SiC nanowires are grown via VLS growth mechanism [62]. In VLS mechanism (see Figure. 2.7), the metal droplet plays the role of a catalyst for decomposing the crystalline species. As the constituents for nanostructures become supersaturated within the liquid alloy, crystal growth proceeds by precipitation of source materials on the solid/liquid interface. Generally, the VLS mechanism leads to high aspect ratio nanostructures, because nucleation and growth process is mainly controlled by the liquid catalyst droplet [63].

Figure 4.4 exhibits SEM image of the SiC nanowires grown at 900 °C with Ni-film catalyst. It is very important to emphasize that high density of SiC nanowires have been achieved at a relatively low temperature of 900 °C with respect to the decomposition temperature of HMDS precursor. The possible reaction scheme for the low temperature deposition of the SiC nanowires from the HMDS precursor can be described as follows: First, HMDS is decomposed at temperatures below 1100 °C and primarily forms $(CH_3)_3Si$ (trimethylsilane) radicals by breaking the silicon-silicon bond. Then, $SiMe_2CH_2$ radical is formed by extracting hydrogen from the $SiMe_3$ [64]. The $SiMe_2CH_2$ radical eliminates CH_4 to form MeSiCH. Then, the MeSiCH radicals could form SiC by undergoing several decomposition steps through eliminating CH_4, C_2H_4, and H_2. Furthermore, the growth of high- density of SiC nanowires at 900 °C suggests that Ni promotes SiC nanowire

formation acting as a very efficient catalyst.

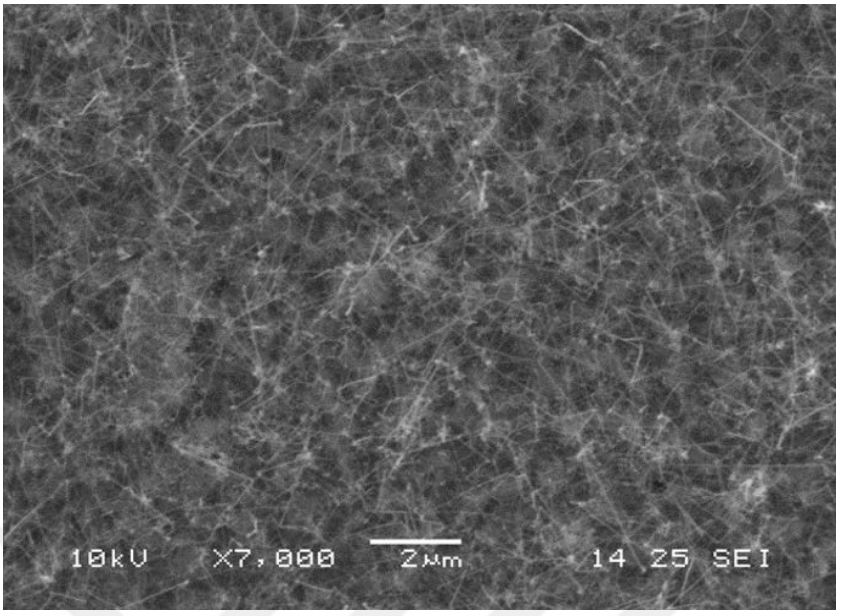

FIGURE 4.4: SEM image of high-density of SiC nanowires synthesized at 900 °C with Ni-film catalyst.

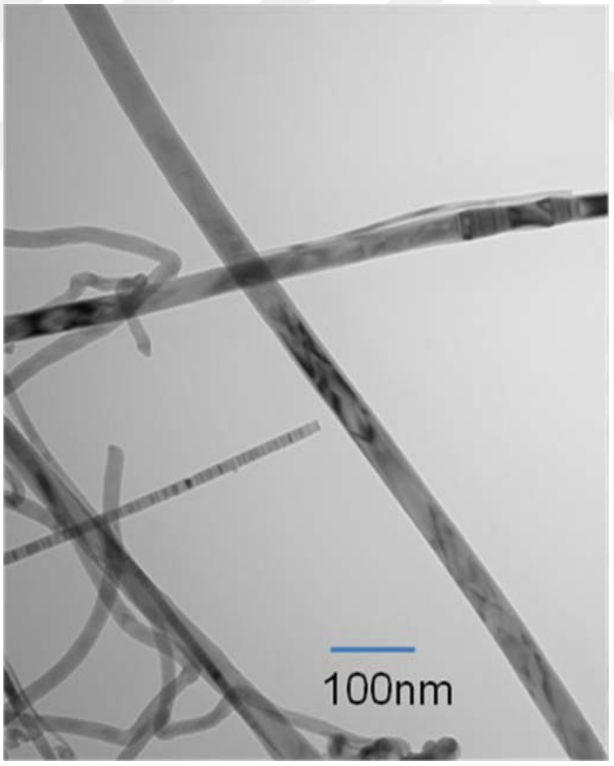

FIGURE 4.5: TEM image of the SiC nanowires exhibiting the diameter ranging from 8 nm to 60 nm.

TEM was employed to characterize the diameter and morphology of the nanowires. The TEM sample was prepared by scraping nanowires from the substrates to the carbon-coated copper grids. Figure 4.5 presents the TEM image of the SiC nanowires with

diameters changing from 8 nm to 60 nm. It is worth mentioning that particularly the straight nanowires have high density of planar defects observed by the dark lines perpendicular to the axis of the nanowires.

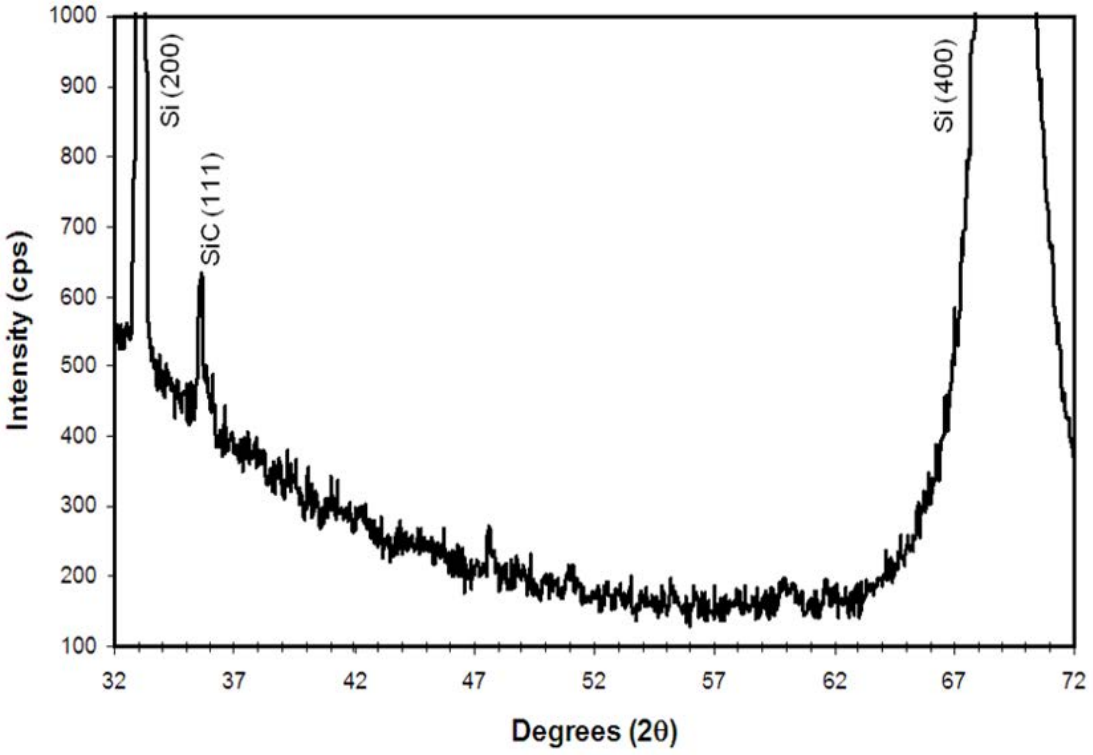

FIGURE 4.6: XRD pattern of the SiC nanowires revealing cubic zinc blende structure (using Cu Kα radiation).

XRD measurements were done using Cu Kα radiation ($\lambda = 0.154$ nm) to determine the crystal structure of the SiC nanowires [63]. And a corresponding spectrum is shown in Figure 4.6. As seen in Figure 4.6, the diffraction peaks in the spectrum were matched to a cubic zinc blende crystal structure. The lattice parameter obtained from the peak position is 0.437 nm, which agree well with the reported values of SiC crystals [JCPDS card No. 29-1129]. The main diffraction peak and its position from SiC nanowires is (111) at 35.65°. Furthermore, the two intense peaks which exist at 32.9° and 69.3° in the diffraction pattern are related to Si substrate. No other crystalline forms or phases was detected in the XRD spectrum [63]. This verifies that the grown SiC nanowires consist of only one crystalline phase with good crystal quality.

4.2 Summary

A simple method to synthesize high quality SiC nanowires was presented. SiC nanowires were directly synthesized by low pressure chemical vapor deposition using HMDS as the source material with various catalyst materials. SiC nanowire growth mechanism VLS and a reaction scheme for the low temperature growth have been discussed.

In summary, high density of SiC nanowires with one crystalline phase have been synsthesized by low pressure chemical vapor deposition at a relative low temperature 900 °C. The nanowires show a uniform morphology with diameters ranging from 8 nm to 60 nm, and it is worth noting that particularly some of the straight nanowires have planar defects observed by the dark lines perpendicular to the axis of the nanowires. Furthermore, the growth of high density of SiC nanowires at 900 °C suggests that Ni substantially promotes SiC nanowire formation acting as a very efficient catalyst.

Chapter 5

Fourier Transform Infrared Spectroscopy Analysis of SiC Nanowires

5.1 Fourier Transform Infrared Spectroscopy

IR spectroscopy provides valuable and practical information about the identification of both organic and inorganic materials. The information about a sample's background, given by each compound's IR spectrum, can be used to characterize unknown materials, as well as to determine molecular structures. An IR spectrum shows detector response and is sketched in absorbance or % transmittance (% T) versus IR frequency (in wave numbers [cm^{-1}]) . A frequency of radiation that interacts with the sample produces an absorption band that is characteristic of the energy required for a particular molecular group. The collective position and pattern of these absorption bands designate the combination of molecular groups found in any specific compound.

Transverse optical (TO) and longitudinal optical (LO) phonon modes determines the infrared radiation optical response of a material in the long wavelength limit. The classification of the mode behaviours depends on oscillator strength of each TO-LO pair [65].

5.1.1 Influence of the Substrate Temperature on SiC Nanowire Phonon Modes

IR absorption of the synthesized nanowire was measured using a FTIR spectroscopy to identify the chemical bonding and chemical nature. Typical FTIR absorption spectra of the as - grown SiC nanowires produced on Si and SiO_2/Si substrate with catalyst iron film is shown in Figure 5.1. The peak positions and FWHM values of the main absorption band of Si-C bond are summarized in Table 5.1.

As shown in Figure 5.1, the spectra of the SiC nanowires revealed the presence of both broad and strong absorption bands with maxima in the ranges of 783 - 793 cm^{-1}, 900 - 970 cm^{-1} and 1060 - 1100 cm^{-1} characteristic of TO Si-C bond, LO Si-C bond , and stretching Si-O bond, respectively.

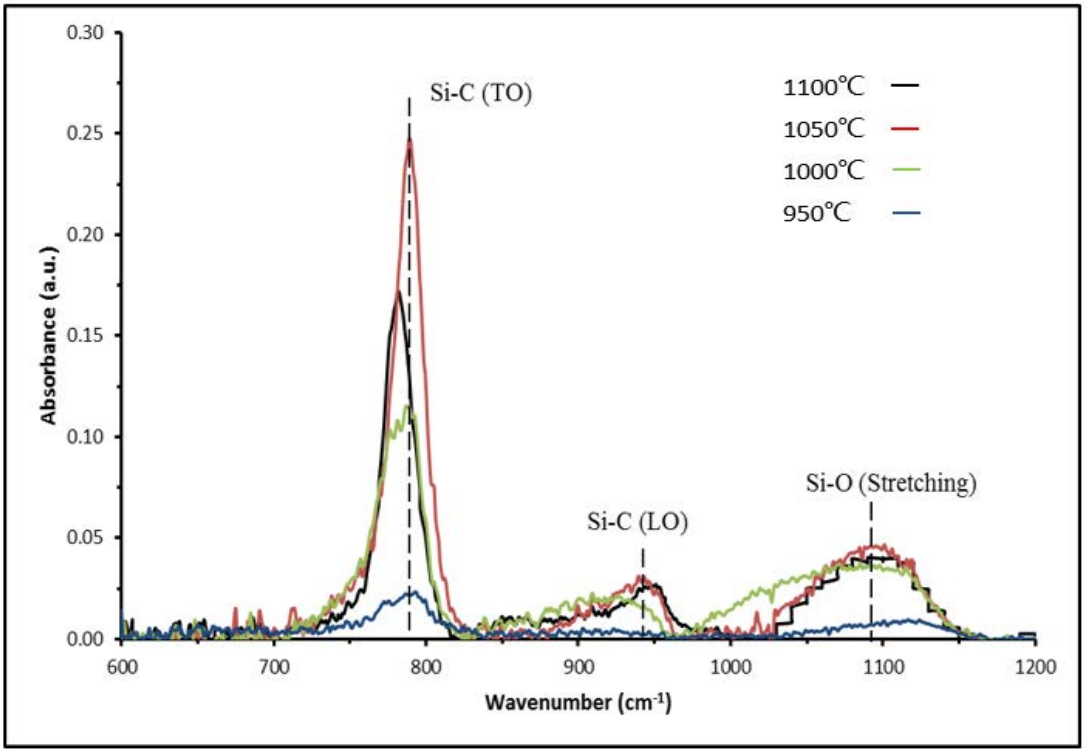

FIGURE 5.1: Infrared spectra of the SiC nanowires grown with catalyst iron film at temperatures of 1100 °C, 1050 °C, 1000 °C, and 950 °C, respectively.

In the first band (783 - 793 cm^{-1}), a strong and sharp absorption peak corresponding to the stretching vibration of the Si-C bond is observed at 783 cm^{-1}, 790 cm^{-1}, 790 cm^{-1}, 793 cm^{-1} at temperature 1100 °C, 1050 °C, 1000 °C, and 950 °C, respectively. It is attributed to the transverse optical phonons of Si-C bonds in SiC nanowires. There is

a small blue shift and broadening of the peak are observed in deposited nanowires with decreasing the growth temperature (as illustrated in Figure 5.1 and Table 5.1).

TABLE 5.1: The peak positions and FWHM values of Si-C TO absorption band.

Growth Temperature	Peak positions of the Si-C bond TO absorption band (cm^{-1})	FWHM values of the Si-C absorption band (cm^{-1})
1100 °C	783	21
1050 °C	790	20
1000 °C	790	27
950 °C	793	36
3C-SiC single crystal[64]	800	59

The changes in the position of the IR absorption of the Si-C bond may arise due to intrinsic stress. The intrinsic stress in the SiC nanowires may induce strain in the chemical bonds of the IR absorber and cause a shift in the frequency of the IR absorption band. The FWHM values of Si-C absorption band increasing from 21 cm^{-1} at temperature of 1100 °C to 36 cm^{-1} for SiC nanowires at temperature 950 °C indicate that the bonding uniformity of the deposited SiC nanowires decreases by reducing the growth temperature. It demonstrates that better chemical order is achieved with higher temperature. Thus, the FWHM value for the SiC peaks decrease with increasing growth temperature of the substrate, because the lattice disorder of SiC was reduced, and the Si-C bonding structure formed high quality crystalline SiC at higher temperature. The Si-C bond in the crystalline configuration leads to a sharp symmetrical absorption band with the peak position being very close to that of single-crystalline 3C-SiC (800 cm^{-1}) [64]. Therefore, an improvement in the crystal quality of SiC nanowires synthesized on SiO_2/Si substrate with catalyst iron film in comparison with the thin single-crystalline 3C-SiC films has been observed. Besides, the peak near 950 cm^{-1} represents the LO stretching Si-C bond; and the peak near 1100 cm^{-1} correspond to stretching mode Si-O bond.

Figure 5.2 shows the FTIR transmission spectra of the SiC nanowires grown on Si substrate with catalyst nickel film at temperatures of 1100 °C, 1050 °C, 1000 °C, and 900 °C, respectively. Table 5.2 shows the peak positions and FWHM values of the main stretching TO Si-C absorption band.

As seen in Figure 5.2, the spectra of the SiC nanowires have shown strong absorption bands with a very small variation. In fact, the TO Si-C bond ranges from 782 to 784 cm^{-1}, the broad LO Si-C bond varies between 930 and 950 cm^{-1}, and the stretching vibration of the Si-O bond locates between 1060 and 1100 cm^{-1}.

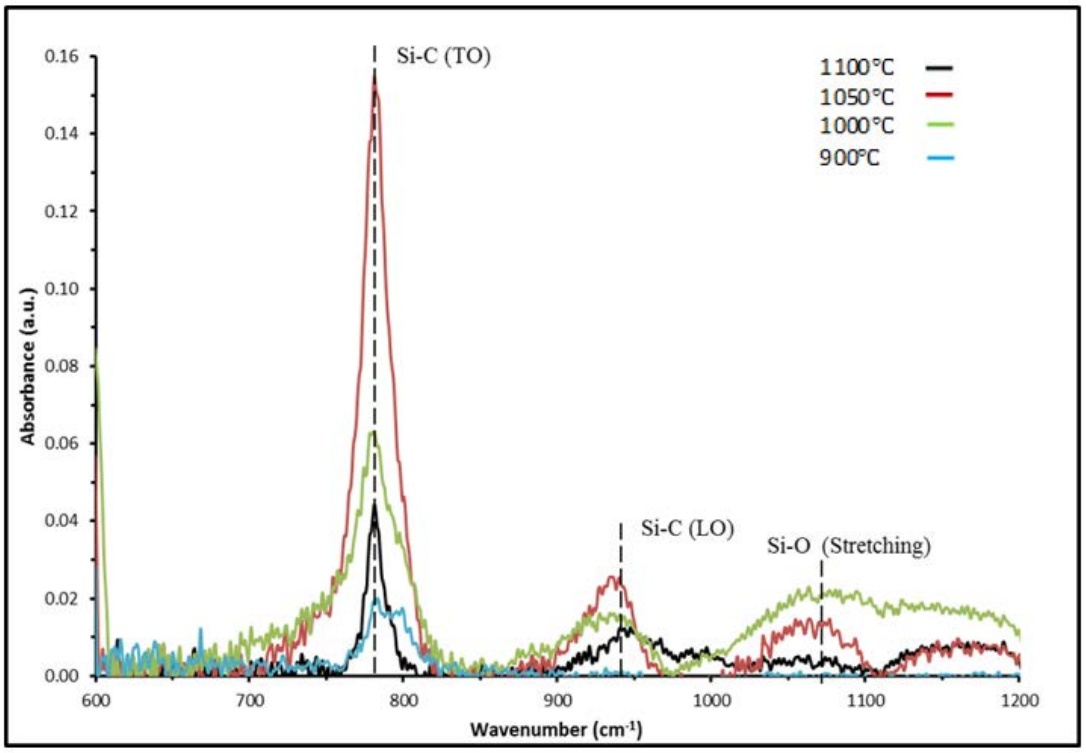

FIGURE 5.2: Infrared spectra of the SiC nanowires grown with catalyst nickel film at temperatures of 1100 °C, 1050 °C, 1000 °C, and 900 °C, respectively.

TABLE 5.2: The peak positions and FWHM values of Si-C TO absorption band.

Growth Temperature	Peak positions of the Si-C bond TO absorption band (cm^{-1})	FWHM values of the Si-C absorption band (cm^{-1})
1100 °C	782	13
1050 °C	782	18
1000 °C	782	22
900 °C	784	31

The FTIR spectra of the SiC nanowires consist of a sharp main band at 780-790 cm^{-1} corresponding to strong absorption bands assigned to the stretching vibration of the Si-C TO bond positioned at about 782 cm^{-1} at the temperatures of 1100 °C, 1050 °C and 1000 °C, and 784 cm^{-1} at 900 °C, respectively. It can be seen that there is no obvious shift, while broadening of the peak is observed as the growth temperature is lowered. As noted in Table 5.2, the FWHM values of the Si-C TO absorption band are increasing ranging from 13 cm^{-1} to 31 cm^{-1} by decreasing the growth temperature. This suggests a slight reduction in the crystal quality of SiC nanowires as the growth temperature is reduced. Therefore, the Si-C bonding uniformity and the crystallinity of SiC nanowires were improved with the increase of the growth temperature. It is important to note that the TO peaks shifted significantly towards the low wavenumber region compared

to the bulk SiC reported earlier, which is 800 cm^{-1} [64]. This could be due to the confinement effects of one-dimensional nanostructures. Moreover, the FWHM values of the SiC nanowires are significantly lower than that of bulk SiC (59 cm^{-1}) [64] indicating better bonding uniformity and crystal quality of the SiC nanowires.

As shown in Figure 5.1 and Figure 5.2, under the same substrate temperature conditions, Si-C TO stretching absorption band ranges approximately from 783 cm^{-1} to 793 cm^{-1} with the FWHM values from 21 cm^{-1} to 36 cm^{-1} on the infrared spectra of SiC nanowires with catalyst iron, while Si-C TO stretching absorption band ranges from 782 cm^{-1} to 784 cm^{-1} with the FWHM values from 13 cm^{-1} to 31 cm^{-1} on the infrared spectra of SiC nanowires with catalyst nickel. It is demonstrated that the FWHM values of the Si-C bond of SiC nanowires produced with catalyst iron is slightly higher than SiC nanowires deposited on substrate with catalyst nickel. This indicates that a slight decrease in bonding uniformity in SiC nanowires formed with catalyst iron. Nevertheless, both Ni and Fe catalysts result in high quality SiC nanowires with very sharp absorption peaks compared to bulk single crystal SiC (FWHM = 59 cm^{-1}) [64].

5.1.2 Phonon Mode Comparison of SiC Nanowires with Different Catalyst Materials at the Same Growth Temperatures

The acquired FTIR spectra of the SiC nanowires using catalyst Fe-film and Ni-film at the same temperature of 1100 °C are shown in Figure 5.3, and the peak positions and FWHM values of the main absorption band of TO Si-C bond are summarized in Table 5.3.

As shown in Figure 5.3, the strong absorption band located at about 783 cm^{-1} for SiC nanowires produced with Fe-film; and 782 cm^{-1} for SiC nanowires produced using Ni-film as a catalyst correspond to the TO Si-C bond. There is no obvious significant shift. The FWHM of Si-C absorption band of SiC nanowires synthesized using Ni-film catalyst is smaller in comparision with SiC nanowires produced with catalyst Fe-film. Therefore, it demonstrates that the grown SiC nanowires with catalyst Ni-film had a very good crystal quality. Fe catalyst also result in high quality SiC nanowires with very sharp absorption peaks.

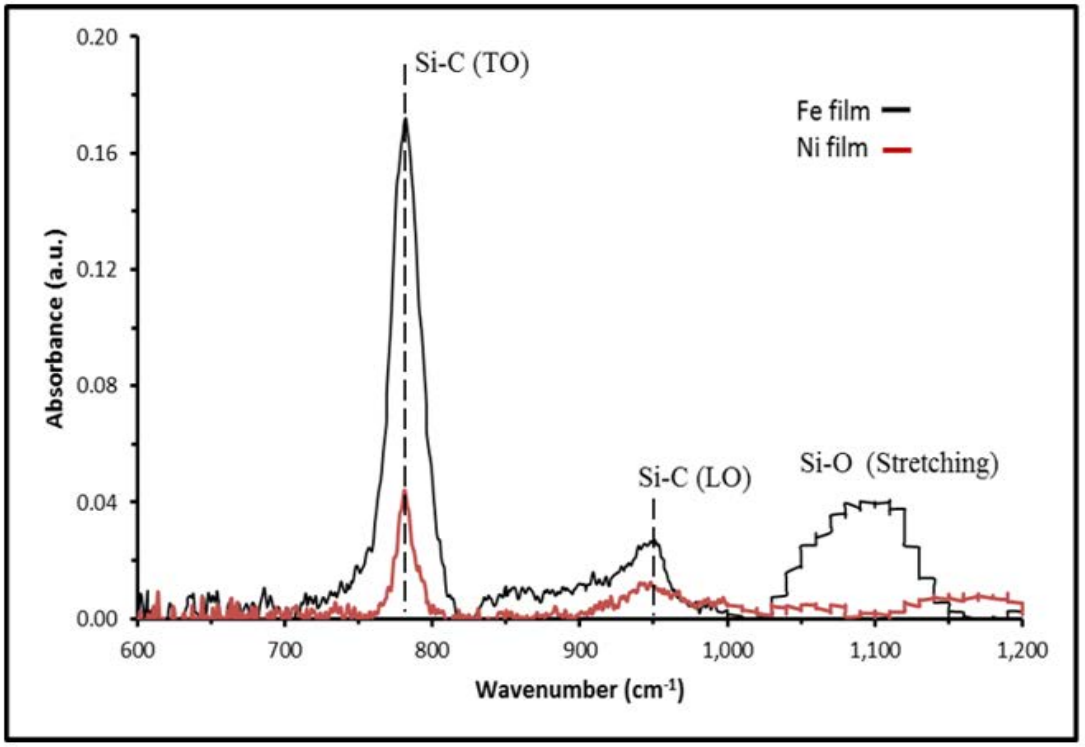

FIGURE 5.3: Infrared spectra of the SiC nanowires grown at a temperature of 1100 °C (a) with catalyst Fe-film, and (b) catalyst Ni-film.

TABLE 5.3: The peak positions and FWHM values of Si-C TO absorption band.

Catalyst type	Peak positions of the Si-C bond (TO) absorption band (cm^{-1})	FWHM values of the Si-C (TO) absorption band (cm^{-1})
Fe film	783	21
Ni film	782	13

The FTIR spectra of SiC nanowires with catalyst Fe-film and the Ni-film at temperature of 1050 °C is shown in Figure 5.4. The FWHM values of the main absorption band of the Si-C bond are summarized in Table 5.4. As shown in Figure 5.4, the strong absorption band located at about 790 cm^{-1} for SiC nanowires produced using Fe-film as a catalyst and 782 cm^{-1} for SiC nanowires produced using Ni-film as a catalyst correspond to the symmetric stretching mode of vibration of the Si-C bond. There is a small variation at the FWHM of the TO absorption band, and the peak position of the TO absorption band shifts to higher wavenumbers in SiC nanowires grown with Fe-film. Both FWHM values are very small and close indicating a very good bonding uniformity and crystal quality of the SiC nanowires. The shift in the peak position of the Si-C stretch may be due to the stress in nanowires formed with catalyst Fe-film.

The measured FTIR spectra of SiC nanowires with using catalyst Fe-film and the catalyst

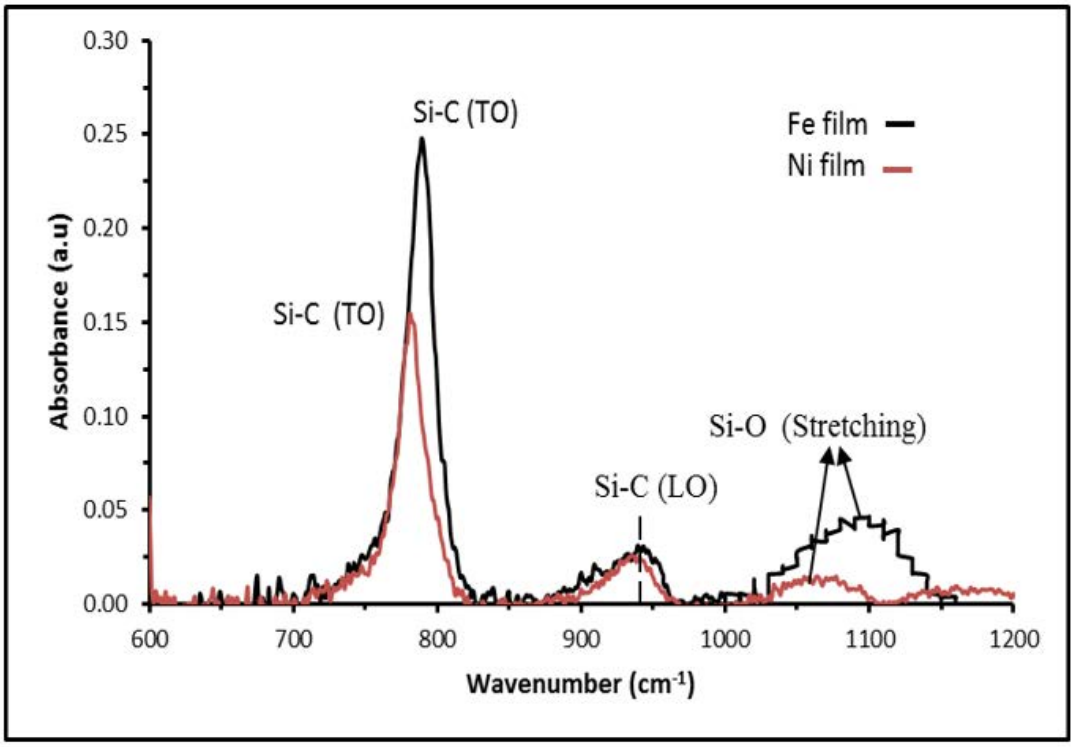

FIGURE 5.4: Infrared spectra of the SiC nanowires grown at a temperature of 1050 °C (a) with catalyst Fe-film, and (b) catalyst Ni-film.

TABLE 5.4: The peak positions and FWHM values of Si-C TO absorption band.

Catalyst type	Peak positions of the Si-C bond (TO) absorption band (cm^{-1})	FWHM values of the Si-C (TO) absorption band (cm^{-1})
Fe film	790	20
Ni film	782	18

Ni-film at the temperature 1000 °C is shown in Figure 5.5. The center peak positions and the FWHM of the main absorption band of Si-C bond are summarized in Table 5.5. As shown in Figure 5.5, the strong absorption band located at about 790 cm^{-1} for SiC nanowires produced using Fe-film as a catalyst with the FWHM value 27 cm^{-1}; and 782 cm^{-1} for SiC nanowires produced using Ni-film as a catalyst correspond to the stretching mode of vibration of the TO Si-C bond with the FWHM value of 22 cm^{-1}. The FWHM of Si-C absorption band of SiC nanowires synthesized using Ni-film catalyst is smaller in comparison to the SiC nanowires produced using Fe-film. Therefore, it suggests that the grown SiC nanowires with catalyst Ni-film have a very good crystal quality and bonding uniformity.

Figure 5.6 shows the FTIR spectra of the SiC nanowires grown at the temperature of 950 °C with catalyst Fe-film and Ni-film, respectively. Table 5.6 shows the center

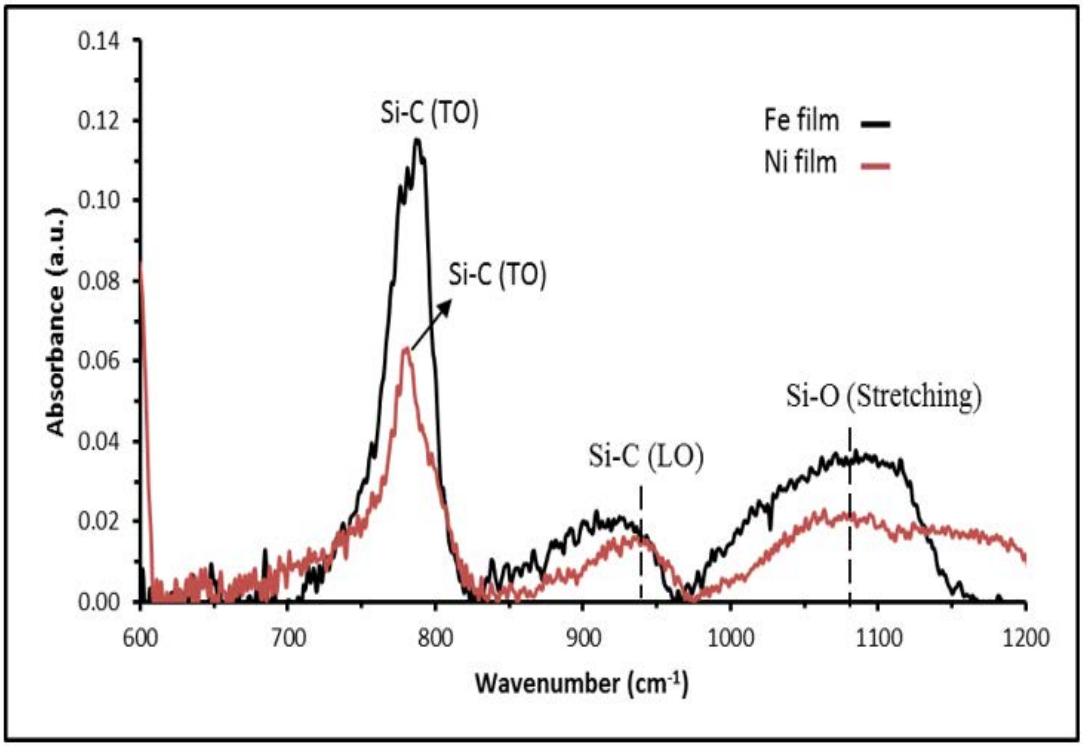

FIGURE 5.5: Infrared spectra of the SiC nanowires grown at a temperature of 1000 °C (a) with catalyst Fe-film, and (b) catalyst Ni-film.

TABLE 5.5: The peak positions and FWHM values of Si-C TO absorption band.

Catalyst type	Peak positions of the Si-C bond (TO) absorption band (cm^{-1})	FWHM values of the Si-C (TO) absorption band (cm^{-1})
Fe film	790	27
Ni film	782	22

positions and FWHM values of the main Si-C absorption band. As seen in Figure 5.6, the spectra of the SiC nanowires revealed the presence of strong absorption band with characteristic of TO Si-C bond, LO Si-C bond and stretching bond Si-O.

As shown in Figure 5.6, the strong absorption band located at about 793 cm^{-1} for SiC nanowires produced with Fe-film as a catalyst, and 797 cm^{-1} for SiC nanowires produced using Ni-film as a catalyst correspond to the stretching mode of vibration of the Si-C bond. It can be seen that there is some broadening of the TO peak. As noted in Table 5.6, the FWHM of Si-C absorption band is higher in SiC nanowires produced with catalyst Fe, which indicates a small degradation in the bonding uniformity and crystal quality of the SiC nanowires. Therefore, the Si-C bonding structure and the crystallinity of SiC nanowires is slightly better with Ni-film as a catalyst.

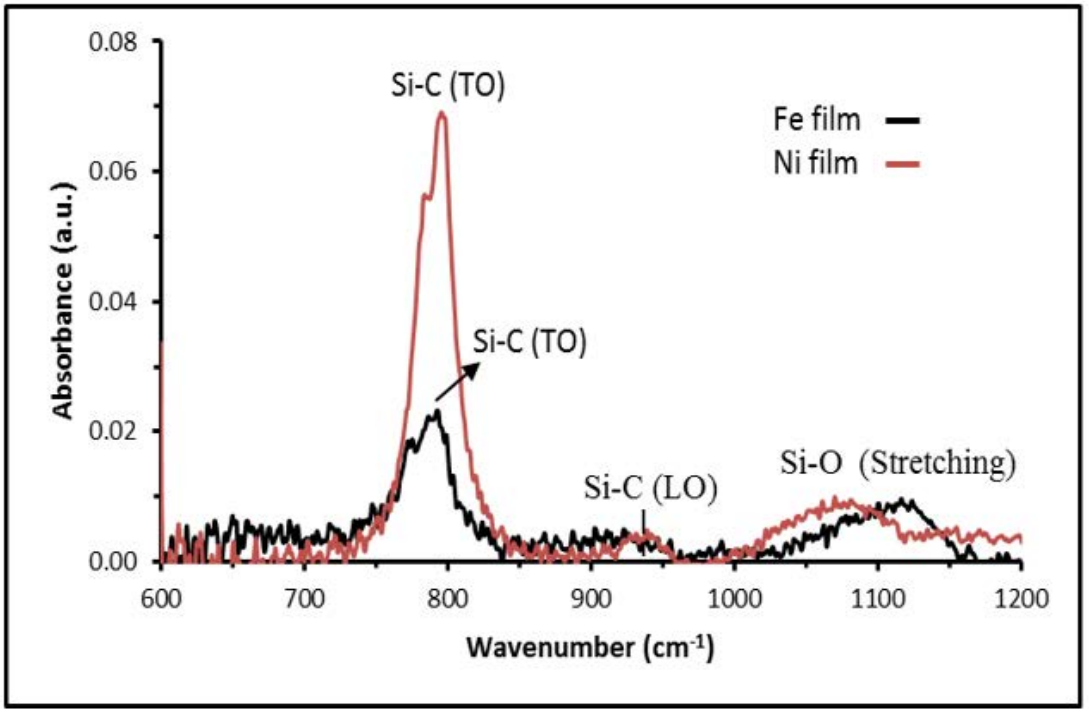

FIGURE 5.6: Infrared spectra of the SiC nanowires grown at a temperature of 950 °C (a) with catalyst Fe-film, and (b) catalyst Ni-film.

TABLE 5.6: The peak positions and FWHM values of Si-C TO absorption band.

Catalyst type	Peak positions of the Si-C bond (TO) absorption band (cm^{-1})	FWHM values of the Si-C (TO) absorption band (cm^{-1})
Fe film	793	36
Ni film	797	30

As shown in Figure 5.7 and Table 5.7, it can be seen that there is no big change in peak position of Si-C absorption band of SiC nanowires synthesized using Ni-film catalyst and Fe-film catalyst at the substrate temperature of 900 °C. As seen in Table 5.7, the FWHM values of the TO Si-C absorption band is higher in SiC nanowires produced using catalyst Fe-film compared to using catalyst Ni-film. Both catalysts Ni-film and Fe-film results in SiC nanowires with low bonding uniformity and crystal quality at lower temperatures.

Figure 5.8 shows FTIR spectra of SiC nanowires grown with Co catalyst. As seen in Figure 5.8, two peaks centered approximately 780-800 cm^{-1} are assigned to stretching vibrations of the Si-C TO mode, peaks centered at about 944 cm^{-1} are attributed to the Si-C LO mode, and two peaks centered around 1070- 1150 cm^{-1} are attributed to stretching mode Si-O bond.

In the first band (780 - 800 cm^{-1}), a strong and sharp absorption peak corresponding

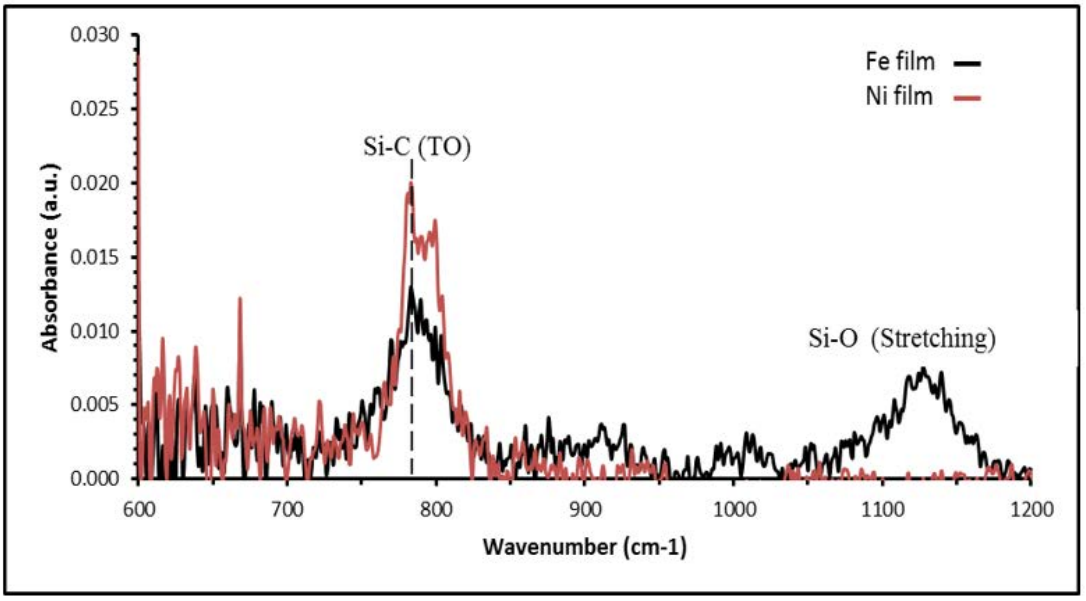

FIGURE 5.7: Infrared spectra of the SiC nanowires grown at a temperature of 900 °C (a) with catalyst Fe-film, and (b) catalyst Ni-film.

TABLE 5.7: The peak positions and FWHM values of Si-C TO absorption band.

Catalyst type	Peak positions of the Si-C bond (TO) absorption band (cm^{-1})	FWHM values of the Si-C (TO) absorption band (cm^{-1})
Fe film	784	35
Ni film	784	31

to the stretching vibration of the Si-C bond is observed at 781 cm^{-1} with the FWHM value of 12 cm^{-1} on SiC nanowires formed on Si substrate with catalyst Co, while the stretching vibration of the Si-C bond is observed at 795 cm^{-1} with the FWHM value of 21 cm^{-1} on SiC nanowires produced on SiO_2 substrate. Although the reason for the small variation for the two different substrate is not clear, small values of the FWHM indicate a very good crystal quality of the SiC nanowires.

TABLE 5.8: The peak positions and FWHM values of Si-C TO absorption band.

Substrate	Peak positions of the Si-C bond (TO) absorption band (cm^{-1})	FWHM values of the Si-C (TO) absorption band (cm^{-1})
Si	781	12
SiO_2	795	21

It is also worth mentioning that a broad SiC LO mode absorption has been observed from the FTIR measurements, that is unique to small size diameter nanowires. Since, electromagnetic waves cannot interact with longitudinal phonons in a large crsytal. However, it is expected to see longitudinal optical resonances from the SiC nanowires, when

the diameter of nanowires is small compared to the incoming wavelength of the radiation [66]. These results show that FTIR provides valuable and more importantly practical information about the chemical bond states and crystal quality of the nanostructured materials.

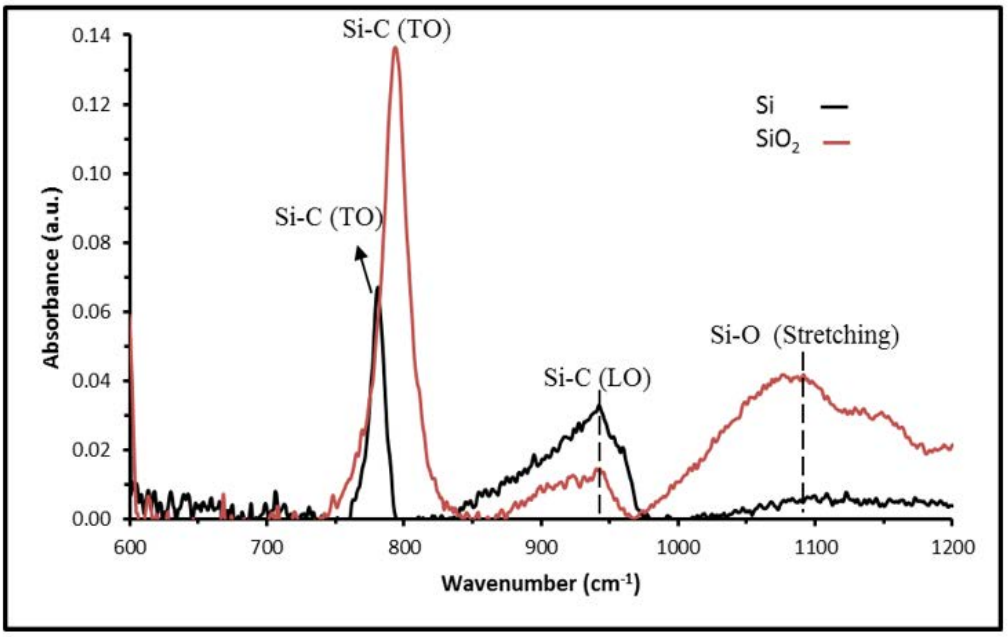

FIGURE 5.8: Infrared spectra of the SiC nanowires grown with catalyst Co at 1100 °C on (a) Si substrate and (b) SiO_2 substrate.

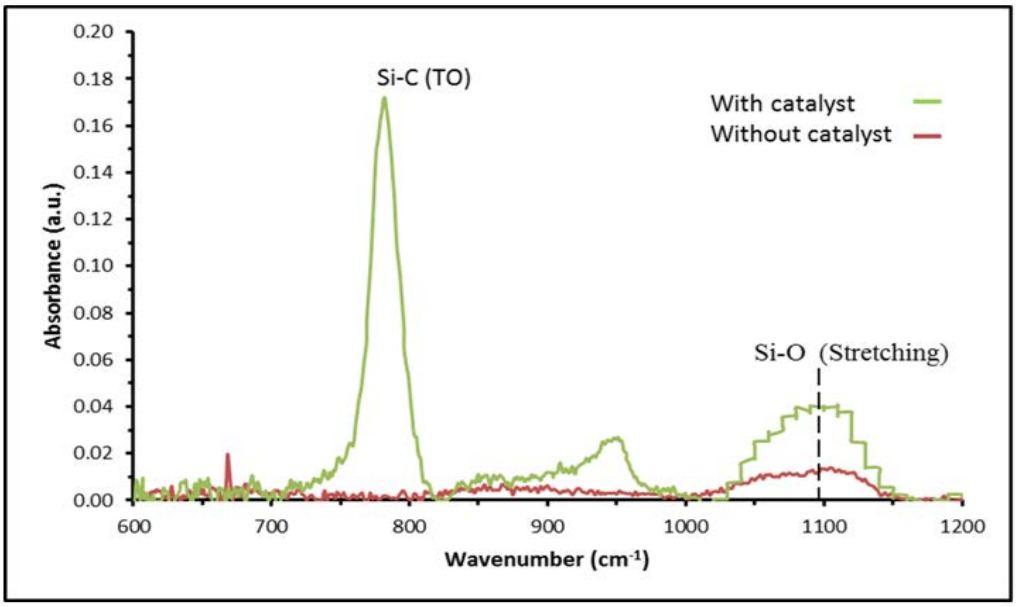

FIGURE 5.9: Infrared spectra of the samples with Fe-catalyst and without any catalyst at the growth temperature of 1100 °C.

In order to evaluate the impact of catalyst on SiC nanowire growth, catalyst free growth experiments have also been caried out. The FTIR spectra of the deposits with and

without any catalyst are shown in Figure 5.9. As shown in Figure 5.9, there is a main peak corresponding Si-C bond with Fe-catalyst for SiC nanowires, while there is no peak observed from the sample without any catalyst. It also demonstrates that catalyst plays an important role to promote the growth of SiC nanowires even at relatively low growth temperatures.

5.2 Summary

An infrared spectrum provides information about identification of a sample with absorption peaks corresponding to the vibrations frequencies between the bonds of atoms. Since each unique composition of atoms makes up different materials, there are no two compounds creating the exact same infrared spectrum. Additionally, the size of the peaks in the spectrum can also be helpful in predicting the amount of material present. Infrared is an excellent valuable tool for quantitative and qualitative analysis of materials.

A comprehensive FTIR spectroscopy investigation of the SiC nanowires grown with various catalyst materials at different temperatures has been provided. Further, the differences of phonon states of SiC nanowires compared to the bulk SiC have been studied. The Si-C TO absorption band ranges from 783 cm^{-1} to 793 cm^{-1} with the FWHM values from 21 cm^{-1} to 36 cm^{-1} with Fe-film catalyst, while the Si-C TO absorption band ranges from 782 cm^{-1} to 784 cm^{-1} with the FWHM values from 13 cm^{-1} to 31 cm^{-1} with Ni-film catalyst. It can be seen that the variation of the Si-C TO peak positions of the SiC nanowires with Fe catalyst is slighly higher than that of with Ni catalyst. Moreover, the FWHM values of the Si-C bond of SiC nanowires with Fe catalyst are slightly higher than that of with Ni catalyst. Nevertheless, both Ni and Fe catalysts result in high quality SiC nanowires with very sharp absorption peaks compared to bulk single crystal SiC (FWHM = 59 cm^{-1}). Additionally, the SiC TO mode absorption shifted significantly towards the low wavenumber region compared to the bulk SiC nanowires.

In addition to the Fe and Ni catalysts, the FTIR measurements were also conducted on SiC nanowires grown with Co catalyst. The results are very similar to the aforementioned catalysts such that strong and sharp absorption peak corresponding to the stretching vibration of the SiC TO mode is observed at 781 cm^{-1} with the FWHM value of 12 cm^{-1} indicating very high crystal quality of SiC nanowires. These results show that

FTIR provides valuable and very practical information about the chemical bond states and crystal quality of the nanostructured materials.

Chapter 6

Conclusions and Future Work

6.1 Conclusions

In this work, a systematic FTIR spectroscopy investigation of the SiC nanowires grown with various catalyst materials at different growth temperatures has been provided. Further, the differences of phonon states of SiC nanowires compared to the bulk SiC have been presented.

FTIR characteristics of SiC nanowires, grown on SiO_2/Si substrate using various catalysts such as iron film, nickel film, and cobalt nanoparticles under temperatures between 900 °C and 1100 °C, showed three strong peaks namely SiC TO mode, SiC LO mode, and Si-O stretching mode. The Si-C TO absorption band ranges from 783 cm^{-1} to 793 cm^{-1} with the FWHM values from 21 cm^{-1} to 36 cm^{-1} with Fe-film catalyst, while the Si-C TO stretching absorption band ranges from 782 cm^{-1} to 784 cm^{-1} with the FWHM values from 13 cm^{-1} to 31 cm^{-1} with Ni-film catalyst. The SiC TO mode absorption shifted significantly towards the lower wavenumber region compared to the wavenumber of bulk single crystal SiC 800 cm^{-1}. These shifts could be due to the quantum confinement effects of the SiC nanowires. In fact, the FWHM values of the TO mode absorption of the grown SiC nanowires are significantly lower than that of bulk SiC (FWHM 59 cm^{-1}). Thus, both Ni and Fe catalysts result in high quality SiC nanowires with very sharp absorption peaks compared to bulk single crystal SiC.

In addition to the Fe and Ni catalysts, the FTIR measurements were also conducted on SiC nanowires grown with Co catalyst. The results are very similar to the aforementioned

catalysts such that strong and sharp absorption peak corresponding to the stretching vibration of the SiC TO mode is observed at 781 cm^{-1} with the FWHM value of 12 cm^{-1} indicating very good bonding uniformity of the SiC nanowires. It is also very important to emphasize that high density of SiC nanowires have been achieved at a relatively low temperature of 900 °C, which is important in integration for various device applications. These results show that FTIR provides a very practical analysis method for providing information about the various chemical bond states and the crystal quality of the nanostructured materials.

6.2 Future Work

In this study, a comprehensive FTIR spectroscopy investigation of SiC nanowires grown by a practical synthesis method using various catalyst materials at different temperatures has been presented. More research effort is needed to design a better-controlled process to synthesize SiC nanowires with desirable diameters, lengths and orientations that could provide a material with greater level of purity, and reduced defect density in order to meet commercial needs and requirements.

One of the greatest challenges is to integrate the SiC nanomaterials (with unique and superior properties) into enriching new applications in nanodevices (sensors, detectors, and actuators), nanowire photonics & optoelectronics, energy, nanocomposites and manufacturing systems. For instance, the SiC-reinforced matrix composites could find applications in aerospace industry and flexible electronics. Additionally, self-assembling nanocircuits made from SiC nanowires could play important roles in future nanodevices for next-generation electronic devices in high temperature and high power applications. Overall, a major challenge is the integration of nanostructured materials for wide range of commercial applications in manufacturing of high-tech products. I strongly believe that future research work will overcome these challenges and introduce these nanostructured materials towards many commercial applications.

Bibliography

[1] H. Seong, H. Choi, S. Lee, J. Lee, and D. Choi. Optical and electrical transport properties in silicon carbide nanowires. *Applied Physics Letters*, 85, 2004.

[2] L. Wang, H. Wada, and L. F. Allard. Synthesis and characterization of SiC whiskers. *Journal of Materials Research*, 7(1):148–163, January 1992.

[3] J. V. Milewski, F. D. Gac, J. J. Petrovic, and S. R. Skaggs. Growth of beta-silicon carbide whiskers by the VLS process. *Journal of Material Science*, 20(4):1160–1166, 1985.

[4] J. Zhu, H. Wu, H. T. Chen, X. L. Wu, and X. Xiong. Tunable violet–blue emission from 3C-SiC nanowires. *Physics Letters A*, 373:1697–1700, 2009.

[5] W. M. Zhou, L. J. Yan, Y. Wang, and Y. F. Zhang. SiC nanowires a photocatalytic nanomaterial. *Physics Letters A*, 89, 2006.

[6] J. J. Niu, J. N. Wang, and Q. F. Xu. Aligned silicon carbide nanowire crossed nets with high superhydrophobicity. *Physical Chemistry B*, 24(13):6918–6923, 2008.

[7] J. J. Niu and J. N. Wang. A novel self-cleaning coating with silicon carbide nanowires. *Physical Chemistry B*, 113(9):2909–2912, 2009.

[8] D. W. Kim, Y. J. Choi, K. J. Choi, J. G. Park, J. H. Park, S. M. Pimenov, V. D. Frolov, N. P. Abanshin, B. I. Gorfinkel, N. M. Rossukanyi, and A. I. Rukovishnikov. Stable field emission performance of SiC-nanowire-based cathodes. *Nanotechnology*, 19(12), 2008.

[9] A. Fujishima and K. Honda. Electrochemical photolysis of water at a semiconductor electrode. *Letters to Nature*, 238:37–38, 1972.

[10] J. Chen, W. Tang, L. Xin, and Q. Shi. Band gap characterization and photoluminescence properties of SiC nanowires. *Applied Physics A*, 102:213–217, 2011.

[11] J. C. Johnson, H. J. Choi, K. P. Knutsen, R. D. Schaller, P. Yang, and R. J. Saykally. Single gallium nitride nanowire lasers. *Nature Materials*, 1(2):106–110, 2002.

[12] P. Yang, H. Yan, S. Mao, R. Russo, J. C. Johnson, R. J. Saykally, N. Morris, J. Pham, R. He, and H. J. Choi. Controlled growth of ZnO nanowires and their optical properties. *Advanced Function Materials*, 12, 2002.

[13] E. W. Wong, P. E. Sheehan, and C. M. Lieber. Nanobeam mechanics: elasticity, strength, and toughness of nanorods and nanotubes. *Science*, 277(5334):1971–1975, 1997.

[14] K. Zekentes and K. Rogdakis. SiC nanowires: material and devices. *Journal of Physics D: Applied Physics*, 44(3), 2011.

[15] T. Burke, K. Xie, J. R. Flemish, R. Singh, T. Podlesak, and J. H. Zhao. Silicon carbide power devices for high temperature, high power density switching applications. *Power Modulator Symposium*, pages 18–21, 1996.

[16] R. C. Clarke and J. W. Palmour. SiC microwave power technologies. *IEEE*, 90(6): 987–992, 2002.

[17] T. Jintakosol, S. Kumfu, P. Singjai, and C. Busabok. Effect of wear tests on silicon carbide nanowires/aluminum metal powder composites. *Chiang Mai Journal of Science*, 39(1):41–48, 2012.

[18] W. Nhuapeng, W. Thamjaree, S. Kumfu, P. Singjai, and T. Tunkasiri. Fabrication and mechanical properties of silicon carbide nanowires/epoxy resin composites. *Current Applied Physics*, 8(3–4):295–299, 2008.

[19] J. A. Powell, P. Pirouz, and W. J. Choyke. Growth and characterization of silicon carbide polytypes for electronic applications. In Z. C. Feng, editor, *Semiconductor Interfaces, Microstructures, and Devices, Properties and Applications*, pages 257–293. CRC Press, Bristol, 1993.

[20] M. Treu, R. Rupp, and P. Blaschitz. Commercial SiC device processing: status and requirements with respect to SiC based power devices. *Superlattices and Microstructures*, 40(4):380–387, October 2006.

[21] J. J. Sha, J. S. Park, T. Hinoki, and A. Kohyama. Bend stress relaxation of advanced SiC-based fibers and its prediction to tensile creep. *Mechanics of Materials*, 39:175–182, 2007.

[22] M. Mehregany and C. A. Zorman. SiC MEMS: opportunities and challenges for applications in harsh environments. *Thin Solid Films*, 355–356:518–524, November 1999.

[23] G. Muller, G. Krotz, and E. Niemann. SiC for sensors and high-temperature electronics. *Sensors and Actuators A: Physical*, 43:259–268, May 1994.

[24] C. M. Zetterling. *Process Technology for Silicon Carbide Devices*. IET, UK, 2002.

[25] M. E. Levinshtein, S. L. Rumyantsev, and M. S. Shur, editors. *Properties of Advanced Semiconductor Materials: GaN, AlN, InN, BN, SiC, SiGe*. Wiley, New York, 2001.

[26] G. S. Chung and K. S. Kim. Heteroepitaxial growth of single 3C-SiC thin films on Si (100) substrates using a single-source precursor of hexamethyldisilane by APCVD. *Bulletin–Korean Chemical Society*, 28(4), April 2007.

[27] A. Watanabe, M. Mukaida, T. Tsunoda, and Y. Imai. Deposits obtained by photolysis of hexamethyldisilane by ArF excimer laser. *Thin Solid Films*, 300(1–2):95–100, May 1997.

[28] J. A. Connor, R. N. Haszeldine, G. J. Leigh, and R. D. Sedgwick. Organosilicon chemistry. part II. The thermal decomposition of hexamethyldisilane, the Me_3Si-$SiMe_3$, bond dissociation energy, and the lonisation potential of the trimethylsilyl radical. *Journal of the Chemical Society A*, January 1967.

[29] W. J. Bullock, R. Walsh, and K. D. King. Very-low-pressure pyrolysis of hexamethyldisilane. kinetic determination of the bond dissociation enthalpy DH° (Me_3Si-$SiMe_3$) and implications for the enthalpy of formation of the trimethylsilyl radical. *Journal of Physics Chemistry*, 98:2595–2601, 1994.

[30] S. Veintemillas, V. Madigou, R. Rodrlguez-Clemente, and A. Figueras. Thermodynamic analysis of metalorganic chemical vapour deposition of SiC using tetramethylsilane as precursor: Identification of the main reactions. *Journal of Crystal Growth*, 148:383–389, 1995.

[31] A. M. Wrobel, A. W. Pietrzykowska, J. E. K. Sapieha, Y. Hatanaka, T. Aoki, and Y. Nakanishi. Remote hydrogen plasma chemical vapor deposition of silicon–carbon thin-film materials from a hexamethyldisilane source: characterization of the process and the deposits. *Journal of Applied Polymer Science*, 2002.

[32] Q. G. Fu, H. J. Li, X. H. Shi, K. Z. Li, J. Wei, and Z. B. Hu. Synthesis of silicon carbide nanowires by CVD without using a metallic catalyst. *Materials Chemistry and Physics*, 100:108–111, 2006.

[33] X. T. Zhou, N. Wang, F. C. K. Au, H. L. Lai, H. Y. Peng, I. Bello, C. S. Lee, and S.T. Lee. Growth and emission properties of beta-SiC nanorods. *Material Science Engineering*, 286(1):119, June 2000.

[34] C. C. Chiu, S. B. Desu, and C. Y. Tsai. Low pressure chemical vapor deposition (LPCVD) of β–SiC on Si (100) using MTS in a hot wall reactor. *Materials Research*, 8(10):2617–2626, 1993.

[35] Z. R. Huang, B. Liang, D. L. Jiang, and S. H. Tan. Preparation of nanocrystal SiC powder by chemical vapour deposition. *Material Science*, 31:4327–4332, 1996.

[36] Z. M. Wang, editor. *One-Dimensional Nanostructurese*. Springer Science and Business Media, New York, 2008.

[37] A. Thess, R. Lee, P. Nikolaev, H. Dai, and P. Petit. Crystalline ropes of metallic carbon nanotubes. *Science*, 273:483–487, 1996.

[38] Y. J. Xing, Q . L. Hang, H. F. Yan, H. Y. Pan, J. Xu, D. P. Yu, Z. H. Xi, Z. Q. Xue, and S. Q. Feng. Solid-liquid-solid (SLS) growth of coaxial nanocables: silicon carbide sheathed with silicon oxide. *Chemical Physics Letters*, 345(1–2):29–32, 2001.

[39] T. H. Yang, C. H. Chen, A. Chatterjee, H. Y. Li, J. T. Lo, C. T. Wu, K. H. Chen, and L. C. Chen. Controlled growth of silicon carbide nanorods by rapid thermal process and their field emission properties. *Chemical Physics Letters*, 379(1–2): 155–161, 2003.

[40] Y. Ryu, Y. Tak, and K. Yong. Direct growth of core-shell SiC-SiO_2 nanowires and field emission characteristics. *Nanotechnology*, 16, 2005.

[41] Z. S. Wu, S. Z. Deng, N. S. Xu, J. Chen, J. Zhou, and J. Chen. Needle-shaped silicon carbide nanowires: Synthesis and filed electron emission properties. *Applied Physics Letter*, 80:3829–3831, 2002.

[42] J. Sarkar, G. G. Khan, and A. Basumallick. Nanowires: properties, applications and synthesis via porous anodic aluminum oxide template. *Bulletin of Materials Science*, 30(3):271–290, 2007.

[43] X. M. Liu and K. F. Yao. Large-scale synthesis and photoluminescence properties of SiC/SiO_X nanocables. *Nanotechnology*, 16:2932–2935, 2005.

[44] C. J. Muller, J. M. van Ruitenbeek, and L. J. de Jongh. Conductance and supercurrent discontinuities in atomic-scale metallic constrictions of variable width. *Physical Review Letters*, 69(140), 1992.

[45] C. J. Muller, J. M. Krans, T. N. Todorov, and M. A. Reed. Quantization effects in the conductance of metallic contacts at room temperature. *Physical Review Letters*, 53, 1996.

[46] B. J. van Wees, H. van Houten, C. W. J. Beenakker, J. G. Williamson, L. P. Kouwenhoven, D. van der Marel, and C. T. Foxon. Quantized conductance of point contacts in a two - dimensional electron gas. *Physical Review Letters*, 60, 1998.

[47] J. L. Costa-Kramer, N. Garcia, and H. Olin. Conductance quantization in bismuth nanowires at 4 K. *Physical Review Letters*, 78, 1997.

[48] W. Yang, H. Araki, A. Kohyama, Y. Katoh, Q. Hu, H. Suzuki, and T. Noda. Tyranno SA/SiC composite with sic nanowires in the matrix by CVI process. *Nuclear Material*, 329:539–543, 2004.

[49] W. Yang, H. Araki, A. Kohyama, S. Thaveethavorn, T. Noda, and H. Suzuki. Fabrication in-situ SiC nanowires/SiC matrix composite by chemical vapour in filtration process. *Material Letter*, 58:3145–3148, 2004.

[50] X. D. Han, Y. F. Zhang, K. Zheng, X. N. Zhang, Z. Zhang, Y. J. Hao, X. Y. Guo, Z. L. Wang, and J. Yuan. Low-temperature in situ large strain plasticity of ceramic SiC nanowires and its atomic-scale mechanism. *Nano Letter*, 7(2):452–457, 2007.

[51] A. Sandhu. Photocatalysis: environmentally friendly SiC nanowires. *Nature Nanotechnology*, 2006.

[52] W. M. Zhou, L. J. Yan, Y. F. Zhang, and Y. Wang. SiC nanowires: A photocatalytic nanomaterial. *Applied Physics Letter*, 89, 2006.

[53] K. Teker. Gallium nitride nanowire devices and photoelectric properties. *Sensors and Actuators A: Physical*, 216:142–146, 2014.

[54] W. Clegg. *Crystal Structure Determination*. Oxford University Press, 1998.

[55] H. Y. Yu. Aluminium nitride nanowires for electronic and photonic applications. Master's thesis, The Hong Kong Polytechnic University, Hong Kong, China, 2010.

[56] D. N. Leonard, G. W. Chandler, and S. Seraphin. Scanning electron microscopy. In *Characterization of Materials*, pages 1–16. Wiley, second edition, October 2012.

[57] A. D. McNaught and A. Wilkinson. *Compendium of Chemical Terminology*. Wiley, 1997.

[58] J. R Markham, P. E Best, and P. R Solomon. Spectroscopic method for measuring surface temperature that is independent of material emissivity, surrounding radiation sources, and instrument calibration. *Applied Spectroscopy*, 48(2):265–270, 1994.

[59] H. Ouyang, P. J. Sherman, E. P. Paschalis, A. L. Boskey, and R. Mendelsohn. Fourier transform infrared microscopic imaging: effects of estrogen and estrogen deficiency on fracture healing in rat femurs. *Applied Spectroscopy*, 58(1):1–9, January 2004.

[60] B. A. Horn, J. Qiu, N. L. Owen, and W. C. Feist. FT-IR studies of weathering effects in western red cedar and southern pine. *Applied spectroscopy*, 48(6):662–668, June 1994.

[61] J. Heberle and C. Zscherp. ATR/FT-IR difference spectroscopy of biological matter with microsecond time resolution. *Applied spectroscopy*, 50(5):588–596, 1996.

[62] R. S. Wagner and W. C. Ellis. Vapor-liquid-solid mechanism of single crystal growth. *Applied Physics Letter*, 4(89), 1964.

[63] K. Teker. Aluminum nitride nanowire array films for nanomanufacturing applications. *Materials Science and Technology*, 31(15):1832–1836, 2015.

[64] F. Yan, Y. D. Zheng, P. Chen, L. Sun, and S. L. Gu. SiC heteroepitaxial growth by low pressure chemical vapor deposition on Si (1 1 1) substrates. *Optical Materials*, 23(1–2):113– 116, 2003.

[65] P. Yew, L. S. Cheong, S. S Ng, Y. T Leong, and H. A Hassan. Theoretical studies on optical phonon and surface phonon polariton of wurtzite AlInN alloys. *Advanced Materials Research*, 1107:565–570, 2015.

[66] R. Kim, W. Qin, G. Wei, G. Wang, L. Wang, D. Zhang, K. Zheng, and N. Liu. Synthesis and properties of SiC/SiO_2 nanochain heterojunctions by microwave method. *Crystal Growth*, 9, 2009.